UNIVERSIDADE DE LISBOA
FACULDADE DE CIÊNCIAS
DEPARTAMENTO DE BIOLOGIA VEGETAL

ISLET AMYLOID POLYPEPTIDE – IAPP – AS A RISK FACTOR FOR DIABETES MELLITUS

FILIPA ISABEL BERNARDO FÉLIX

Mestrado em Biologia Molecular e Genética

Dissertação orientada por:
Doutora Regina Menezes
Doutor Manuel Carmo Gomes

[2018]

i. Acknowledgements

Gostaria de deixar um especial agradecimento a todos os que me acompanharam e contribuiram para a realização da minha tese de mestrado. Nomear todos os que perderam o seu tempo para me aconselhar e para me incentivar seria impossível, mas estou certa de que sem as pessoas que me acompanharam durante todos estes meses, tudo seria mais complicado.

Em primeiro lugar, sou muito grata à Drª Cláudia Santos por me ter recebido no MNH e por todas as palavras de confiança nos momentos mais dificeis.

Gostaria de agradecer à minha orientadora Drª Regina Menezes por toda a atenção, tempo e paciência disponibilizada, pois teria sido para mim impossível realizar este trabalho sem as suas palavras de incentivo e esclarecimentos. A si devo-lhe todas as conquistas deste ano!

Gostaria de agradecer ao meu orientador Drº Manuel do Carmo Gomes por toda a atenção disponibilizada, a prontidão em ajudar e por todos os esclarecimentos.

Apesar de breve, a minha passagem pela APDP foi de uma enorme satisfição e estou muito grata pela disponibilidade e amabilidade de todas as pessoas que me receberam como uma verdadeira colega.

Quero agradecer especialmente às meninas do MNH, Inês Figueira, Andreia Gomes, Rita Ramos, Joana Pereira e Paula Pinto por toda a ajuda disponibilizada, pelas indicações preciosas e, sobretudo pela boa disposição, pois fizeram-me rir muitas vezes mesmo em momentos mais complicados.

Gostaria de agradecer às minhas colegas de mestrado, Catarina Bastos e Marcela Vaz que sempre me ajudaram e incentivaram a enfrentar os problemas de frente. Foi um prazer ser vossa colega!

Aos meus amigos, pela compreensão na minha ausência e pelo carinho e força que me transmitiram na minha presença. Sem o vosso apoio, este meu percurso teria sido muito mais duro.

Quero agradecer, sobretudo à minha família, que sempre me incentivou a perseguir os meus sonhos e sempre me fizeram acreditar que seria capaz de atingir todos os meus objectivos. Sem a vossa confiança e respeito eu não seria a pessoa que sou hoje.

O meu muito obrigada a todos!!!!

ii. Abstract

The accumulation of amyloid deposits in the pancreas is a histopathological hallmark of type 2 diabetes. Evidences suggest that intermediate oligomeric species, rather than the amyloid structures primarily composed of the Islet Amyloid Polypeptide (IAPP) hormone, contribute to β-cell dysfunction and loss.

Human IAPP (hIAPP) is an amyloidogenic polypeptide expressed in pancreatic β-cells as a proprotein. IAPP and insulin are co-expressed, processed by the same enzymes and co-secreted in response to the same cellular stimulus, leading to the concerted regulation of their activity towards whole-body glucose homeostasis. The molecular mechanisms underlying hIAPP intracellular oligomerization leading to the accumulation of amyloid plaques in the pancreas is still poorly understood. Humanized yeast models of IAPP expression were previously constructed to facilitate the investigation of the intracellular effects of IAPP. With the goal to overcome limitations of the previous models, this study intended to construct improved models by integrating the cDNA encoding for mature and unprocessed hIAPP forms into the genome, the latter referred as the most amyloidogenic species. The construction of novel models allowed the investigation of the cytotoxic properties of hIAPP forms, revealing that overexpression of proIAPP more drastically impaired cellular growth and led to the accumulation of hIAPP aggregates in the vacuole. In addition, the models were shown to be valuable tools to investigate hIAPP processing as convertase activity is evolutionary conserved.

hIAPP expressed in the pancreas circulates in the bloodstream being distributed to target tissues. Since the accumulation of hIAPP oligomers precedes the deposition of pancreatic amyloids, it was hypothesized that detection of hIAPP oligomers in the plasma could serve as an early indicator of diabetes. Preliminary analyses indicated the presence of ~22-24 kDa signal potentially representing hIAPP oligomers in the plasma sample of a volunteer diagnosed with diabetes. Further studies are required to address the significance of these results.

Keywords: diabetes, IAPP, IAPP oligomerization, IAPP processing, yeast

iii. Resumo

A Diabetes mellitus (DM) é definida como uma desordem metabólica caraterizada por hiperglicemia crónica e alterações no metabolismo de glícidos, lípidos e proteínas devido à insuficiente secreção e/ou ação de insulina. A DM pode ser dividida em duas grandes classes: a Diabetes tipo 1 (T1DM) que engloba 5-10% dos casos de doença e carateriza-se pela ocorrência da destruição auto imune das células β do pâncreas. A segunda classe denomina-se de diabetes tipo 2 (T2DM), inclui 90-95% dos indivíduos com diabetes e neste caso existe uma insuficiente secreção de insulina e/ ou resistência à sua ação. A T2DM pode persistir sem diagnóstico por muitos anos até ser detetada e consequentemente estes indivíduos apresentam um elevado risco de desenvolvimento de complicações macrovasculares e microvasculares. Na realidade, em 2015 estimou-se que 13,3% da população portuguesa entre os 20 e 79 anos de idade sofriam de T2DM e 44% destas pessoas ainda não tinham obtido um diagnóstico. A elevada prevalência, complexidade clínica e natureza crónica da DM representam um enorme encargo médico e socioeconómico tornando urgente o desenvolvimento de novas estratégias de diagnóstico e de terapia.

Uma das caraterísticas frequentemente observadas nas autópsias de indivíduos com T2DM é a presença de depósitos amilóides no pâncreas e as evidências sugerem que os agregados tóxicos de uma proteína denominada Polipéptido Amilóide dos Ilhéus (IAPP) contribuem para a disfunção e a perda das células β pancreáticas. A IAPP é uma proteína neuro-endócrina de 37 resíduos de aminoácidos, codificada por um gene localizado no cromossoma 12 em humanos e expresso nas células β pancreáticas. O péptido é expresso, armazenado e secretado em resposta aos mesmos estímulos que a insulina e embora a sua função ainda não seja clara, é reconhecido um papel na homeostase da glucose. A sequência imatura de IAPP é uma pré-proproteína composta por 89 resíduos de aminoácidos - pré-proIAPP (ppIAPP) - cujo péptido sinal é hidrolisado no retículo endoplasmático (ER). Após remoção do péptido sinal, a proIAPP (pIAPP), uma pro-proteína de 67 resíduos, sofre a ação das mesmas enzimas responsáveis pelo processamento de proinsulina a insulina: prohormona convertase 1/3 (PC 1/3) e prohormona convertase 2 (PC2) para a formação da proteína madura – IAPP.

Apenas os humanos, primatas não humanos e gatos expressam uma proteína altamente amiloidogénica, contrariamente ao que acontece com os roedores. Uma diferença em apenas seis resíduos de aminoácidos torna a proteína humana susceptível à oligomerização, em oposição ao que acontece com os roedores. A existência de regiões amilodoigénicas no péptido, a sobreexpressão da proteína como consequência do aumento da expressão de insulina (resultado da resistência periférica à sua ação) e erros no processamento das formas imaturas da proteína são fatores que podem ser associados à formação de agregados de IAPP. No entanto, os mecanismos moleculares que desencadeiam a agregação da proteína ainda não são totalmente conhecidos.

A levedura *Saccharomyces cerevisiae* é um organismo eucariota frequentemente utilizado como modelo experimental. Possui um sistema genético bem definido, é de fácil manipulação, não patogénico e a sua utilização apresenta custos relativamente baixos. Alguns dos processos celulares fundamentais são conservados entre a levedura e os humanos e cerca de 31% dos genes da levedura possuem homólogos em mamíferos. Este organismo é frequentemente utilizado para estudar processos biológicos complexos como a replicação de DNA, progressão do ciclo celular, transdução de sinal e outros mecanismos relevantes. Mesmo os genes humanos que não possuem um homólogo em levedura podem ser estudados neste organismo, através de expressão heteróloga, para dar origem aos denominados modelos de leveduras humanizadas. Estes modelos eucariotas foram já validados para o estudo de algumas doenças neurodegenerativas, como a doença de Parkinson e conseguem recapitular algumas das caraterísticas da doença. Assim, foram previamente desenvolvidos modelos de levedura que expressam a forma humana de ppIAPP (pphIAPP), pIAPP (phIAPP) e IAPP (hIAPP) marcadas com GFP (*green fluorescent protein*) utilizando vetores episssomais de múltiplas cópias. No entanto, a

instabilidade destes vetores gera artefactos técnicos que dificultam a interpretação dos resultados. Para contornar esta limitação, neste estudo foram desenvolvidos modelos optimizados de expressão do IAPP através da integração do cDNA que codifica para o hIAPP, phIAPP and pphIAPP no genoma da levedura. Estes modelos são valiosos para a investigação das propriedades citotóxicas da proteína madura e imatura, que representou o segundo objectivo deste estudo.

Uma das principais conclusões deste trabalho é que, tal como acontece na agregação da α-sinucleína, uma cópia do gene de pphIAPP e phIAPP é insuficiente para que o crescimento da levedura seja comprometido, apesar de a sua expressão afectar alguns parâmetros de crescimento como a duração da fase *lag*, que reflete o tempo necessário para a duplicação celular, e a biomassa final. No caso das células que expressam hIAPP o crescimento demonstrou ser ligeiramente afetado pela expressão da proteína mas a citoxicidade foi bastante inferior aos resultados obtidos com as estirpes que expressam os vetores de múltiplas cópias. Posto isto, o modelo foi optimizado através da introdução de uma segunda cópia do respetivo cDNA no genoma das estirpes recombinantes. A expressão de duas cópias da construção de phIAPP foi suficiente para que a maioria dos parâmetros relacionados ao crescimento celular fossem afetados. Mais, as estirpes foram sujeitas a ensaios de microscopia de fluorescência onde foram detetados sinais de stress celular, como a presença de largos vacúolos nas células, associados à expressão destas proteínas. A expressão de duas cópias de phIAPP teve um impacto mais drástico no crescimento celular e levou ainda à acumulação de agregados no vacúolo. Curiosamente, não foi possível detetar a proteína pphIAPP nos ensaios de microscopia de fluorescência, o que pode sugerir que o transcrito desta proteína possa ser instável ou que a proteína possa ser degradada como estratégia de defesa celular. Ensaios adicionais são necessários para corroborar esta hipótese. A expressão das formas não processadas de hIAPP foi testada por *immunoblotting* e os resultados indicam a presença de diversos intermediários de processamento sugerindo que convertases endógenas processam a pphIAPP, o que pode ocasionar a remoção do *tag* de GFP.

A presença de agregados de IAPP nas células β do pâncreas está bem documentada. Estes agregados foram não só detetados no pâncreas dos indivíduos, mas também em outros órgãos, nomeadamente nos rins de indivíduos com nefropatia diabética e no coração de pessoas com excesso de peso e/ou obesidade e em indivíduos diagnosticados com T2DM. Estes depósitos podem ser correlacionados com o dano nos tecidos onde se encontram. Depósitos da proteína podem ser também encontrados no cérebro de indivíduos diagnosticados com a doença de Alzheimer ou demência e simultaneamente de T2DM. Uma vez que as espécies oligoméricas de IAPP presentes no cérebro parecem ser transportadas a nível circulatório e o nível de expressão de IAPP no cérebro é muito baixo, é sugerido que oligómeros de IAPP expressos no pâncreas possam circular na corrente sanguínea e alojar-se em diferentes órgãos com consequências nefastas para os tecidos. De fato, foram já detetados tetrâmeros de IAPP em amostras de plasma humano. Este é um resultado importante para a exploração dos oligómeros de hIAPP como um potencial indicador da diabetes. Desta forma, foram realizados diversos ensaios para a deteção de oligómeros de IAPP no plasma de voluntários saudáveis e em voluntário diagnosticado com diabetes. Através da utilização de um anticorpo que reconhece o epítopo dos resíduos 20-29 da hIAPP foi detectado um sinal de cerca de 22-24 kDa que pode efectivamente corresponder a oligómeros hIAPP.

Palavras-Chave: diabetes, IAPP, oligomerização de IAPP, processamento de IAPP, levedura.

iv. Index

v. Table Index

vi. Figures Index

vii. List of abbreviations, symbols, chemical formulas and units

AIC	Akaike information criterion
AGE	Advanced glycation end products
APS	Ammonium persulfate
AUC	Area under the curve
BSA	Bovine serum albumin
Ca^{2+}	Calcium
CEN	Centromere
cDNA	Complementary DNA
CGRP	Calcitonin gene-related peptide
CHOP	CCAA-enhancer-binding protein homologous protein
COOH	Carboxyl
COS-1	Kidney fibroblast-like cell line
CPE	Carboxypeptidase E
CSM	Complete supplement mixture
C-terminal	Carboxyl-terminal
DAPI	4',6-Diamidine-2'-phenylindole dihydrochloride
DM	Diabetes mellitus
E	Empty vector
ER	Endoplasmic reticulum
E. coli	*Escherichia coli*
g	g-force
g	gram
G	Glycine
Gal	Galactose
GFP	Green fluorescent protein
Glu	Glucose
gt	Generation time
h	Hour
HCl	Hydrochloric acid
hIAPP	Human Islet Amyloid Polypeptide
His18	Histidine 18
H_2O	Water
IAPP	Islet Amyloid Polypeptide
IDE	Insulin degrading enzyme
IL-1β	Interleukin 1β
INS-1	Insulin secreting beta cell derived line
K	Lysine
KCl	Potassium chloride
KDa	Kilodalton
L	Liter
LADA	Latent autoimmune diabetes in adults
LB	Luria-Bertani
LiAc	Lithium acetate
M	Molar
$MgCl_2$	Magnesium chloride
$MgSO_4$	Magnesium sulfate
min	Minute
mL	Milliliter

NaCl	Sodium chloride
ng	Nanograme
NH_2	Amine
N-terminal	Amine-terminal
OD	Optical density
ODi	Initial optical density
PAGE	Polyacrylamide gel electrophoresis
PAM	Peptidyl amidating mono-oxygenase
PBS	Phosphate buffered saline
PC1/3	Prohormone convertase 1/3
PC2	Prohormone convertase 2
PEG	Polyethylene glycol
Pgk1	3-Phosphoglyceric phosphokinase
phIAPP	Pro human -Islet amyloid Polypeptide
pIAPP	Pro-Islet Amyloid Polypeptide
PMD	Protein misfolding disorder
pphIAPP	Pre pro human-Islet Amyloid Polypeptide
ppIAPP	Pre pro-Islet Amyloid Polypeptide
PVDF	Polyvinylidene fluoride
R	Arginine
rIAPP	Rodent Islet Amyloid Polypeptide
ROS	Reactive oxygen species
rpm	Rotation per minute
s	Second
SD	Synthetic defined
SDS	Sodium dodecyl sulfate
Ser28	Serine 28
SOC	Super optimal broth with catabolite repression
S. cerevisiae	*Saccharomyces cerevisiae*
S1	Plasma sample 1
S2	Plasma sample 2
S3	Plasma sample 3
S4	Plasma sample 4
S5	Plasma sample 5
t	Time
TAE	Tris base; acetic acid; EDTA
TBS	Tris buffered saline
TBS-T	Tris buffered saline plus tween 20
TCA	Trichloroacetic acid
TE	Tris EDTA
TEMED	Tetramethylethylenediamine
Trp	Tryptophan
T1DM	Type 1 diabetes mellitus
T2DM	Type 2 diabetes mellitus
UCH-L1	Ubiquitin carboxyl-terminal hydrolase
UPS	Ubiquitin proteasome system
Ura	Uracil
V	Volt
Vf	Final volume
Vi	Initial volume
XBP1	X-box binding protein 1

YNB	Yeast nitrogen base
YPD	Yeast extract; peptone; glucose
2μ	2 micron
ºC	Celsius degree
μg	Microgram
μL	Microliter

1. Theoretical fundaments

1.1 Diabetes mellitus

Diabetes mellitus (DM) is defined as a metabolic disorder whose main features are chronic hyperglycemia and alterations in the metabolism of carbohydrates, fat and protein due to a deficiency in insulin secretion and/or action[1]. DM is majorly classified in Type 1 diabetes mellitus (T1DM) and Type 2 diabetes mellitus (T2DM). T1DM or "juvenile-onset diabetes" comprises 5-10% of DM patients and is characterized by the autoimmune destruction of pancreatic β-cells. The rate of β-cell loss is variable, being fast in some individuals (generally infants and children) and slow in others. T2DM, also named "adult-onset diabetes", includes 90-95% of DM cases[2]. These patients have relative insulin deficiency and peripheral insulin resistance[3]. Whereas total islet mass is greatly reduced in T1DM, islet loss in T2DM is a gradual process and individuals may not need insulin treatment to survive[4]. This form of DM can persist undiagnosed for many years until hyperglycemia can be detected, consequently, these patients have an increased risk of developing macro- and microvascular complications[1]. In 2015, the estimated prevalence of T2DM in the Portuguese population, aged between 20 and 79 years (7.7 million individuals), was of 13.3% with a significant difference between men (15.9%) and women (10.9%). 56% of these individuals had already been diagnosed but 44% didn't have a diagnosis[5]. The high prevalence, clinical complexity and chronic nature of DM are the main causes of the huge medical and socioeconomic burden of the disease[6].

1.2 Diabetes as a protein misfolding disorder

Protein misfolding disorders (PMDs) refer to a set of diseases sharing the misfolding, aggregation and accumulation of proteins as a pathological hallmark. Aggregates of specific proteins can be found as intracellular inclusions or extracellular plaques (amyloid structures), which can cause cellular damage and ultimately tissue and organ dysfunction[6,7]. Although the proteins associated with different PMDs are structurally and chemically different, the resulting aggregates and amyloids are very similar, being organized in a cross β-sheet quaternary structure. These structures have also similar properties as resistance to proteolysis, capacity to bind to dyes as Congo Red and thioflavin S, and fibrillar aspect in electron microscopy[7].

At least fifty different PMDs have been characterized, including neurodegenerative diseases, diverse systemic disorders, certain forms of heart disease, cancer and T2DM[8,9].

Amyloid deposits in the islets of Langerhans is a pathological hallmark of T2DM, being often observed in autopsy samples from patients[8,10] and evidences suggest that toxic aggregates of a pancreatic hormone called Islet Amyloid Polypeptide (IAPP)[11] or amylin[12] may contribute to β-cell dysfunction and loss[13,14].

1.2.1 Physiological role of IAPP

IAPP is a 37 amino acid neuroendocrine peptide displaying homology with calcitonin gene-related peptide (CGRP). It is encoded by a single-copy gene localized on human chromosome 12, which is highly expressed in pancreatic β-cells[15]. Insulin and IAPP genes contain related promoter elements[16,17], being therefore expressed in response to similar stimulus[18]. The protein is stored, along with insulin, in secretory granules, and secreted in response to the same secretagogues[18,19]. In general, like insulin, the plasma levels of IAPP are lower in the fasting state and rise in the post prandial state[20].

Although the physiological functions of IAPP remain largely unknown, it's recognized that this protein has a complementary action to insulin playing an important role on glucose homeostasis. IAPP affects the glucose levels in the bloodstream by (1) signaling the stomach to slow gastric emptying, delaying the absorption of glucose from the small intestine into the circulation and (2)

stimulating the satiation center of the brain thus limiting nutrient intake[20,21]. IAPP also prevents the release of glucose from liver cells acting on arginine induced glucagon secretion. It was suggested that the protein does not act on the pancreatic cells but possibly in central nervous system[22].

1.2.2 IAPP processing and clearance

IAPP is expressed as a larger precursor, preproIAPP (ppIAPP), of 89 amino acid residues (Figure 1.1). It contains a NH_2 terminal signal-sequence, which is cleaved in the Endoplasmic reticulum (ER), generating the 67 amino acid propeptide proIAPP (pIAPP)[23,24]. The processing of pIAPP in β-cells is initiated by the cleavage of its COOH terminus by the prohormone convertase 1/3 (PC1/3)[25]. In the absence of PC1/3, pIAPP COOH-terminus processing is catalyzed by prohormone convertase 2 (PC2)[25,26]. The remaining dibasic residues, the lysine (K) and arginine (R), are then removed by the carboxypeptidase E (CPE)[27]. Final processing of the COOH terminus involves removal of the exposed glycine (G) and amidation of the tyrosine by the Peptidyl amidating mono-oxygenase complex (PAM)[27]. The NH_2 terminally unprocessed intermediate pIAPP is cleaved in secretory granules by PC2[26]. In addition, a disulfide bridge between cysteine residue 2 and 7 is essential for IAPP full biological activity[12,15]. It is noteworthy to mention that, besides sharing the same regulatory elements, the enzymes responsible for pIAPP processing are the same that process proinsulin to insulin[24], tightly connecting the activity of both hormones.

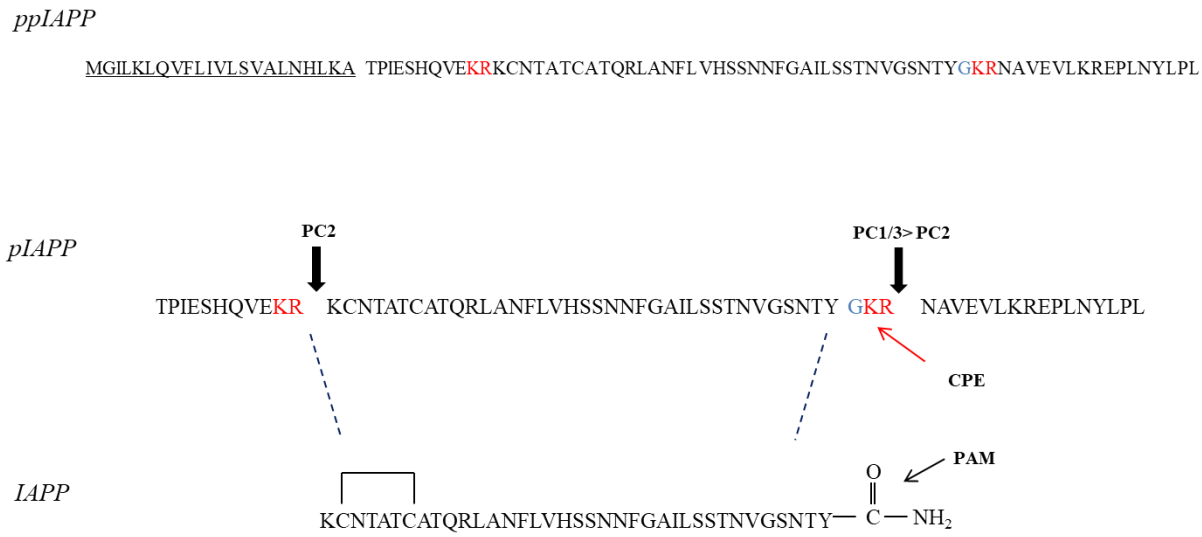

Figure 1.1 Schematic representation of IAPP processing. The ppIAPP 22-amino acid signal peptide (underlined) is cleaved off in the ER. pIAPP processing is initiated in the COOH terminus preferentially by the action of PC1/3. The KR residues (red) that remain at COOH terminus are removed by CPE. The glycine residue (blue) is then removed and the PAM complex catalyzes the amidation of the COOH terminus. The cleavage of the NH2 terminus by PC2 yields the mature IAPP. For full biological activity a disulfide bridge between cysteine 2 and 7 is formed. ppIAPP – preproIAPP; pIAPP – proIAPP; PC1/3 -Prohormone convertase 1/3; PC2 - Prohormone convertase; CPE - Carboxypeptidase E; PAM - Peptidyl amidating mono-oxygenase complex. Adapted from Akter et al., 2015[111].

IAPP is cleared from plasma by renal excretion[28], however there are other alternative systems for IAPP removal. The Insulin degrading enzyme (IDE) is a protease responsible for degradation of IAPP and insulin, although it presents a lower affinity for IAPP than for insulin[29]. Another protease involved in IAPP removal is neprilysin. It is a type II zinc-containing metalloprotease that degrades IAPP[30] and also inhibits the formation of IAPP fibrils by a non-catalytic mechanism[31].

1.2.3 IAPP amyloidogenic properties and islet amyloid formation

The amino acid sequence of IAPP is highly conserved but there are interspecific differences critical for amyloid formation (Figure 1.2). Only humans[32], non-human primates[33] and cats[34] express a

highly amyloidogenic protein. Conversely, rodents (mouse and rat) and several other mammalian species express a form of IAPP lacking amyloidogenic properties[32].

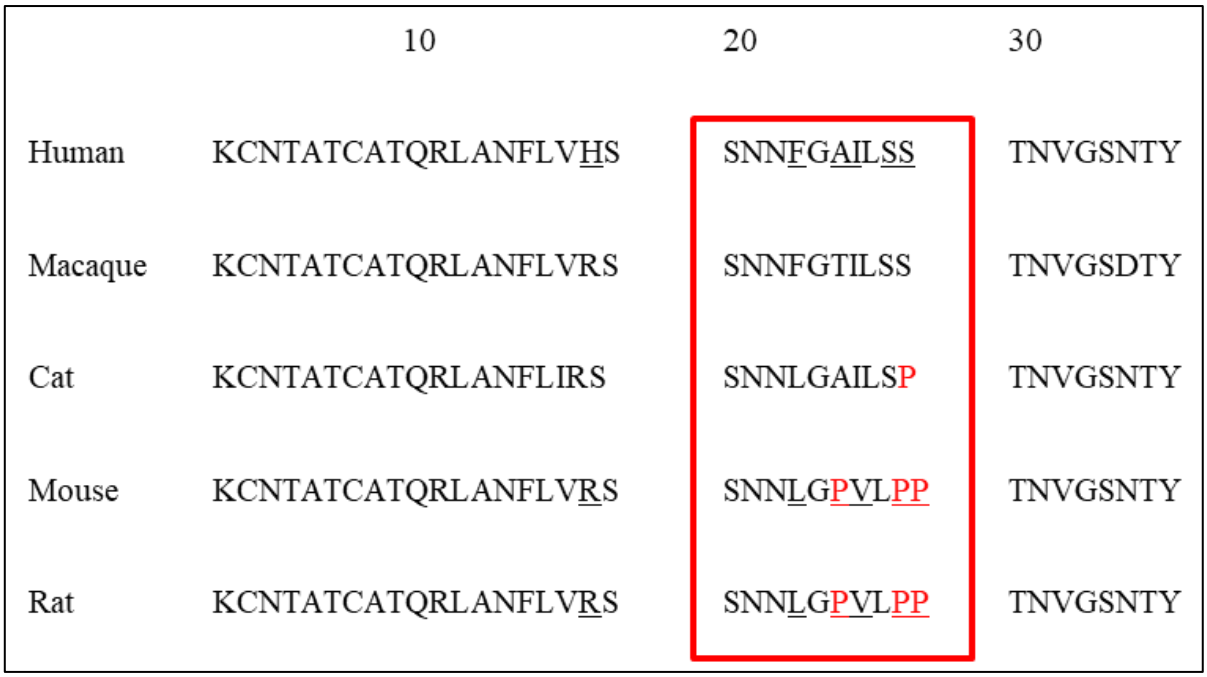

Figure 1.2 Comparison of IAPP amino acid sequences from mammalian species. IAPP sequences are highly conserved but exhibit notable differences in the region between the amino acid residues 20-29 (red box). Non-conserved amino acids are underlined and the β-sheet breaker residues proline (P) are indicated (red). Adapted from Westermark *et al*., 2011[112]

Interspecific variations in IAPP primary structure seem to be responsible for the different amyloidogenic propensity of each form. Most of them occur between the residues 20-29, where five out of six differences can be observed in the IAPP sequences from humans and rodents (Figure 1.2). Indeed, i*n vitro* experiments in which human IAPP (hIAPP) single amino acids were substituted by rodent amino acids between the residues 20 to 29 influenced amyloid fibril formation negatively. Rodents contain proline residues at positions 25, 28, 29, which disrupt the β-sheet conformation. In fact, exchanging the Ser28 by a proline in hIAPP most dramatically inhibited aggregation[32]. Even though this region is determinant for amyloid formation, two other potentially amyloidogenic domains have also been described: 30–37[35] region and 8–20 region[36,37]. The first domain is 100% identical in hIAPP and rodent IAPP (rIAPP). The only difference observed in the second domain is the substitution of hIAPP His18 by an arginine in rodents. Although both hIAPP and rIAPP possess two potentially amyloidogenic domains[36], the proline rich domain (residues 20-29) observed in rodent sequences may inhibit an intramolecular conformation required for amyloid formation[36] (Figure 1.3).

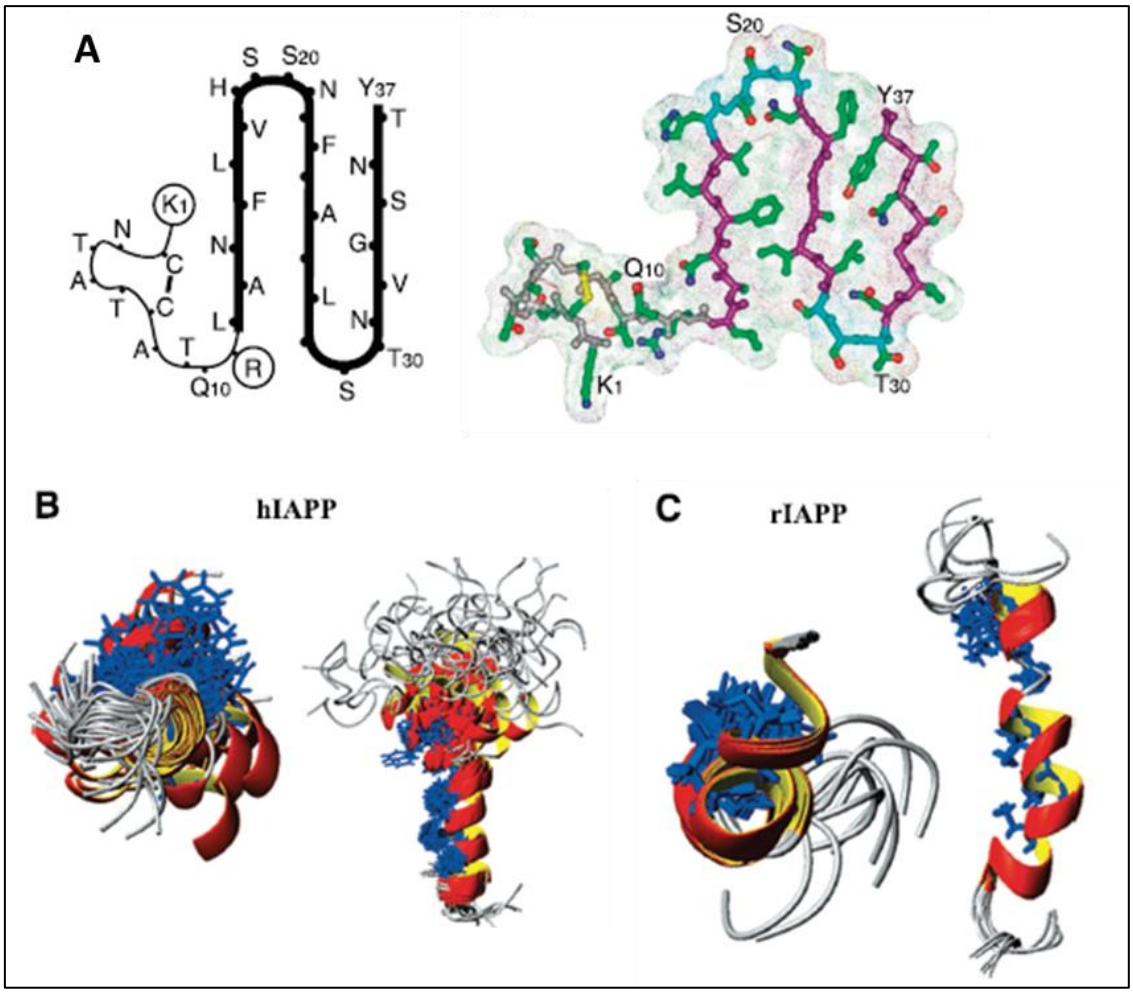

Figure 1.3 Structure of human and rat IAPP. A) Proposed model of hIAPP in the β-serpentine fold with the indication of three β-strands. The first 11 amino acid residues contain a disulfide-bonded loop, which is incompatible with extending the serpentine on this side (left). Ball-and-stick representation of the β-serpentine model. The backbones of the β-strands are represented in purple and the loops in blue (right). Adapted from Kajava *et al*, 2005[38]. B) Three dimensional structure of hIAPP and (C) rIAPP in the presence of dodecylphosphocholine micelles. hIAPP and rIAPP have both an ordered helical structure at NH_2 terminus and distorted COOH terminus. The rIAPP has a rigid NH_2 terminus that is bent toward of amphipathic helix whereas the NH_2 terminus of hIAPP is more flexible. hIAPP – human IAPP; rIAPP – rodent IAPP. Adapted from Nanga *et al*., 2009[39].

The molecular triggers for hIAPP fibril formation are not yet known. The presence of the amyloidogenic regions is one associated issue. The fact that fibrilization does not happen in all individuals suggests that there are cellular mechanisms ensuring the proper hIAPP folding to a monomeric form. Several *in vitro* studies suggested that the environment of the secretory vesicles favors the correct conformation of hIAPP and that insulin is a potent inhibitor of fibril formation. Changes such as hIAPP overexpression, as a consequence of insulin resistance, may disrupt the homeostasis of the vesicles resulting in hIAPP aggregation[40,41]. However, overexpression of hIAPP in the first transgenic mice models proved to be insufficient for amyloid formation suggesting that additional factors must influence amyloid deposition in T2DM[42,43].

The impairment of hIAPP degradation system has been also associated with amyloid formation. In conditions where hIAPP levels exceed the degradation capacity of IDE, either by increased hIAPP expression or decreased expression or activity of IDE, the balance change from degradation to deposition[29]. This is clearly illustrated by the notion that insulinoma cell models treated with exogenous hIAPP, in which IDE was inhibited with bacitracin, amyloid formation and cell toxicity were increased[44].

T2DM is associated with chronically hyperglycemia and oxidative stress[45], which contribute to the formation of Advanced glycation end products (AGE). Evidences have shown that AGE modification converts hIAPP into a higher amyloidogenic form than the unmodified peptide[46].

Increased ratios of secreted proinsinsulin/insulin are observed in T2DM and both hIAPP and insulin are processed by the action of the same enzymes, PC1/3 and PC2[24,47]. Thus, it is plausible to consider that inefficient pro-hIAPP (phIAPP) processing also occurs in T2DM. It was demonstrated that phIAPP has the typical properties of an amyloidogenic peptide[48] and there is immunological evidence for the presence of phIAPP in amyloid deposits[24,49]. Consequently, the increase of phIAPP levels may contribute to islet amyloid deposition[13]. According to these evidences, it is suggested that β-cell dysfunction is associated with folding and/or trafficking impairment resulting in the increase of misfolded/unprocessed hIAPP in the secretory vesicles. The release of these hIAPP forms from the vesicles may expose them to an environment promoting additional structural changes favoring fibril formation. Besides, misfolded phIAPP/hIAPP in secretory granules may induce the granule contents to be targeted to lysosomal degradation[50]. This argues that amyloid formation starts intracellularly, with the fibrils being released into the extracellular space after cell death. Once these fibrils are formed, they provide the seed required to the amyloid accumulation[13].

1.2.4 Mechanisms of toxicity

Several mechanisms of hIAPP-induced toxicity have been proposed although the exact causes of β-cell death are still unclear. Initially, it was thought that large fibrils were the most pathological species that triggers the disease, but a growing number of evidences indicate that soluble oligomers are the cytotoxic agents[51].

Membrane permeabilization by toxic oligomers is one of the proposed mechanisms. It has been reported that hIAPP oligomers form pore-like structures in cell membranes, such as the ER and mitochondria and the plasma membrane as well (Figure 1.4). Nonselective plasma membrane leakage occurs followed by Ca^{2+} dysregulation and hyper-activation of calpain[52]. Calpain belongs to a cytosolic cysteine proteinase family that requires Ca^{2+} for activity and plays a role in various biological processes as cell migration, cytoskeletal remodeling, cell differentiation and apoptosis. Studies in cells exposed to hIAPP aggregates also indicate the loss of mitochondrial membrane potential, ATP depletion and other mitochondrial associated damage[53]. The intracellular accumulation of protein aggregates are known to produce chronic stress beyond the capacity of the ER, potentially leading to cellular death by inducing CHOP and caspases (Figure 1.4). In fact, it was shown that increased expression of hIAPP in INS-1 cells and transgenic rats leads to ER stress–induced apoptosis[54].

Chronic inflammation may be a significant factor in amyloid toxicity and it is frequently observed in local and systemic amyloidosis. hIAPP aggregates can contribute to cell dysfunction triggering a localized inflammatory response by stimulating the inflammasome and consequently IL-1β, which is thought to play a direct role in hIAPP induced β-cell dysfunction and death[55,56] (Figure 1.4). In addition to this notion, it was observed that the internalization of IAPP aggregates by resident macrophages in pancreatic tissue secrete multiple inflammatory cytokines, including IL-1β[57].

Elevated levels of hIAPP may also reduce the efficiency of the Ubiquitin Proteasome System (UPS), responsible to target numerous cellular proteins for degradation. Studies in human islets have shown that increased hIAPP levels downregulate, by unknown mechanisms, the expression of Ubiquitin Carboxyl-terminal hydrolase (UCH-L1), an enzyme essential for proteolytic degradation by the proteasome (Figure 1.4). Impaired UPS response may ultimately lead to aggregation and toxicity[58].

There are also evidences that hIAPP aggregates in transgenic mice impairs lysosome-dependent degradation in β-cells that may lead to cell apoptosis (Figure 1.4), although the mechanisms of impairment is still unknown[59].

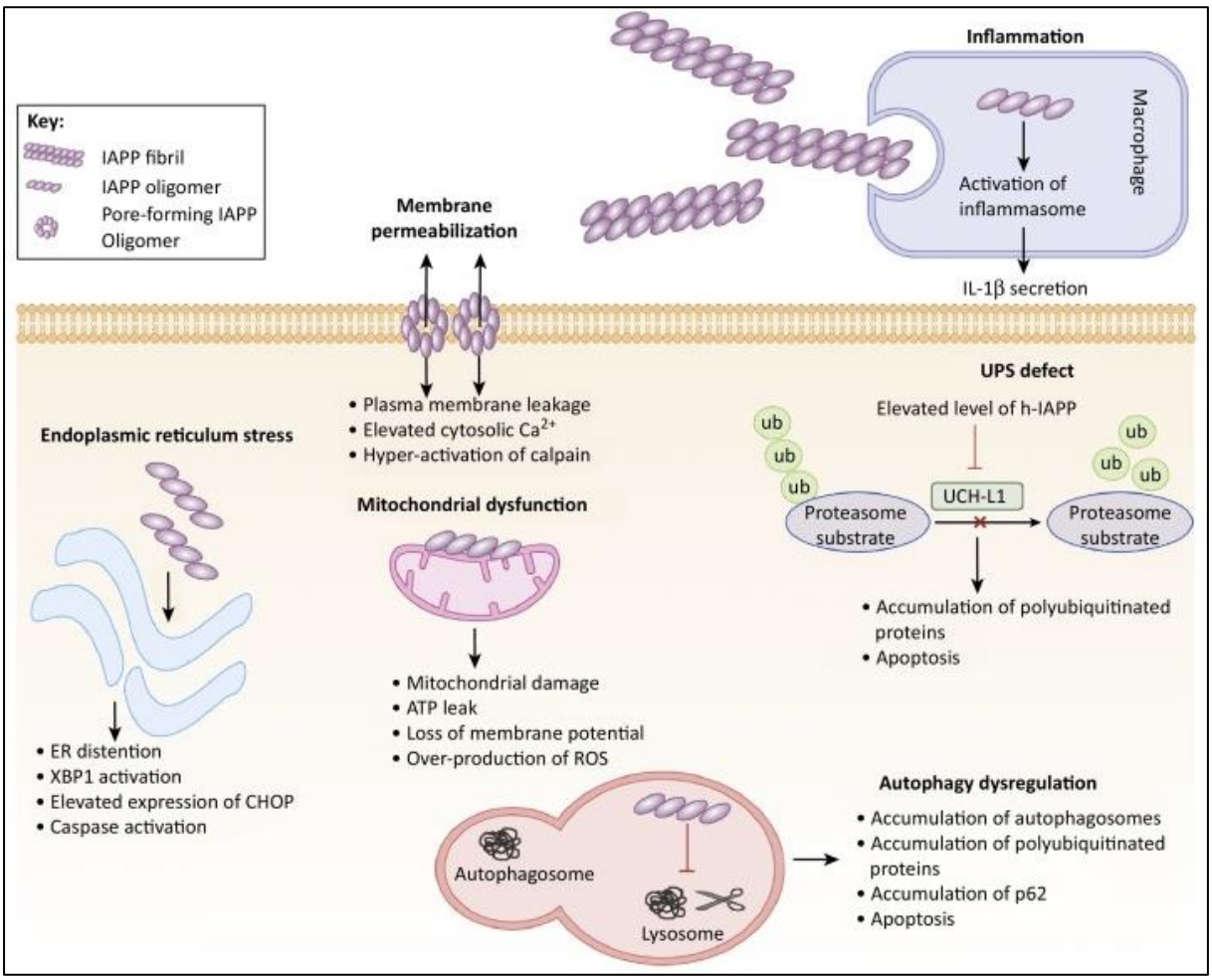

Figure 1.4 Molecular mechanisms of IAPP-induced toxicity. hIAPP oligomers induce membrane permeabilization, impair the function of ER, mitochondria, UPS and autophagy and trigger inflammatory responses. ER – Endoplasmic reticulum; Ub – ubiquitin; XBP1 - X-box binding protein 1; CHOP - CCAAT-enhancer-binding protein homologous protein; ROS - Reactive oxygen species; UCH-L1 - Ubiquitin carboxy-terminal hydrolase L1; hIAPP – human IAPP. Adapted from Mukherjee *et al*., 2015[113].

1.2.5 Role of islet amyloid in diabetes

The dysfunction and loss of β-cells are key features of T2DM and attributed to several factors including glucolipotoxicity, inflammation, accumulation of cholesterol and islet amyloid formation[60]. The cytotoxic properties of IAPP are well described, however, the role of IAPP amyloids in DM onset and progression is still a subject of discussion[61,62]. It is not yet clear whether the formation of IAPP amyloids is a cause or a consequence of T2DM but it is proposed that hyperinsulinemia, accompanied by high levels of IAPP, promotes IAPP oligomerization. This pathological process ultimately may also contribute to the development of insulin insufficiency by promoting the β-cell failure[63].

IAPP amyloid deposition may as well reduce β-cell replication and it was proposed that replicating cells are more vulnerable to apoptosis induced by small oligomers of hIAPP[64]. It was also shown that hIAPP amyloids are associated with decline of β-cell replication in transplanted graft of transgenic mice, explaining at least partially the non-immune loss of β-cells and recurrence of hyperglycemia following islet transplantation[65].

Although IAPP amyloids are most commonly associated with T2DM, it was recently shown that a group of children and adolescents with classical T1DM have high IAPP concentrations in plasma at the clinical onset of the disease. Hence, it is speculated that increased IAPP levels may also be a risk factor for oligomerization and β-cell destruction in T1DM[66].

Oligomerized IAPP accumulates not only in pancreas but as well in the kidneys of patients with diabetic nephropathy. It was described the presence of IAPP aggregates in kidney biopsies being the deposition well correlated with disease severity and it is suggested that renal IAPP deposition may contribute to diabetic renal lesion[67].

IAPP deposits were also detected in the heart of obese and T2DM individuals and it was proposed that this accumulation accelerates the development of cardiac dysfunction[68]. High levels of small IAPP aggregates have been also found in non-failing hearts from overweight and obese individuals indicating that cardiac IAPP deposition may start in early phases of insulin resistance and pre-diabetes[68].

In other study it was demonstrated that IAPP accumulates in the brain and in both blood vessels and perivascular spaces of patients suffering from Alzheimer's disease or dementia and T2DM. A curious outcome of the study is the finding of IAPP deposits in the brain of Alzheimer's disease patients without diabetes suggesting that these patients may suffer from insulin resistance[69]. IAPP oligomers deposit in the brain as independent plaques or co-precipitates with amyloid-β. For this reason IAPP has been considered a second amyloid contributing to the pathology of age-related neurodegenerative disorders[69].

The absence of IAPP transcripts in human brain indicates that IAPP is not locally expressed, instead it is assumed that IAPP expressed in the pancreas circulates in the bloodstream being thus distributed to target tissues. Indeed, it was possible to detect IAPP tetramers in plasma samples of patients by immunoblotting[69]. This is an important result that supports the exploitation of IAPP oligomers as a biomarker for early DM diagnosis. Another aspect that should be considered is the consequences of IAPP over secretion as a result of treatments stimulating insulin production[70].

1.3 Experimental models of IAPP aggregation and amyloid formation

Several spontaneous and genetically modified animal models have been used to study the consequences of IAPP amyloid formation. Non-human primates are the closest to humans whereas domestic cats have also been used as they develop diabetes associated with the deposition of IAPP. In both models, it was demonstrated that IAPP deposition precedes the fasting hyperglycemia in animals with impaired glucose tolerance[71,72]. These models have provided strong evidences that IAPP deposits early in the pathogenesis of T2DM. However, the use of these animal models is very expensive and challenging so several lines of transgenic mice expressing hIAPP have been developed. As observed in humans, the expression of amyloidogenic IAPP forms in mice is not by itself enough to induce islet amyloid formation[43,73], even though one group had described that small deposits of fibrillary material were present within the secretory granules[74]. The initial studies with these mice were performed in a normal metabolic environment and these observations strongly suggested that the presence of impaired β-cell function is required for amyloid fibril formation. In fact, IAPP amyloid formation is promoted by inducing obesity and/or insulin resistance in these models[75,76].

Transgenic mice have been valuable models to understand the consequences of IAPP amyloid formation. Nevertheless, more amenable models are required to deep investigate the molecular mechanisms underlying IAPP-induced β-cell dysfunction. Mammalian cells represent a suitable model to study hIAPP aggregation and the mechanism of intracellular oligomerization. A study using transfected COS-1 cells established that high levels of hIAPP expression, but not rIAPP, results in intracellular aggregation[77]. These results were in agreement with *in vitro* studies showing that hIAPP amyloid fibrils are cytotoxic to human and rat islet cells[62]. Even though pancreatic β-cells from mammalians represent a valuable model to IAPP oligomerization, their use is limited by the highly specialized culture conditions[78].

1.4 Yeast as a protein misfolding disorder model

The yeast *Saccharomyces cerevisiae* is a commonly used eukaryotic model organism whose genome can be easily manipulated. The features that make yeast a versatile experimental system include a well-defined genetic system, rapid growth, ease of plating and mutant isolation, and a highly versatile DNA transformation system. In addition, yeast is a nonpathogenic organism that provides a cheap source for studying complex biological processes[79]. Yeast allowed the clarification of basic cellular mechanisms as DNA replication, cell cycle progression, protein turnover, vesicular trafficking, signal transduction and mechanisms involved in longevity and cell death[80]. The fundamental cellular processes are well conserved between yeast and humans and about 31% of the yeast genes have a mammalian homologue[81]. In addition, about 30% of human disease genes known to be involved in human diseases may have a yeast orthologue[81,82] . In turn, human genes that do not have a yeast orthologue can be heterologous expressed originating the so called humanized yeast models[83].

PMDs differ in their pathophysiology but share a common feature that is the accumulation of protein aggregates. Protein folding is a critical process for the maintenance of life, thus intricate cellular mechanisms, conserved from yeast to humans, have evolved to ensure that proteins are correctly folded[84]. Thus, yeast can provide a valuable tool to explore the mechanisms behind aberrant protein aggregation[85]. Humanized yeast models expressing disease proteins associated with PMDs have allowed major advances in the understanding of the fundamental pathological processes of human diseases[86,87]. Many aspects of hIAPP proteotoxicity remain to be elucidated and yeast models emerge as useful tools to address the molecular mechanisms underpinning hIAPP oligomerization.

A yeast model of hIAPP aggregation was developed (Menezes *et al*., unpublished data) to support the study of hIAPP pathophysiology. The humanized IAPP yeast models consist of the fusion of the cDNA corresponding to unprocessed and processed IAPP forms fused to Green fluorescent protein (GFP) inserted in the backbone of the episomal vector pRS426 (Figure 4.1). Expression of the chimeric proteins is regulated by the yeast *GAL1* promoter, allowing tight repression by glucose and ready activation in the presence of galactose[88]. Preliminary data indicate that hIAPP overexpression in yeast recapitulates the formation of intracellular aggregates and cytotoxicity, observed in mammalian cells, supporting the use of these models to investigate the fundamental mechanisms of hIAPP proteotoxicity and to screen for protective molecules.

2. Aims

The study had three major goals:

(1) The optimization of humanized yeast model of IAPP oligomerization through the integration of human ppIAPP and pIAPP constructs into the yeast genome;
(2) The investigation of the cytotoxic properties of mature and unprocessed hIAPP forms;
(3) The evaluation of hIAPP oligomers as a potential indicator of diabetes.

3. Materials and Methods

3.1 Bacterial strain and growth conditions

Escherichia coli (*E. coli*) [*recA1endA1 gyrA96 thi-1 hsdR17 supE44 relA1 lacI* [F'*proAB lacIqZDM15 Tn10 (Tet$_r$)]* was used for cloning purposes and plasmid propagation. Cells were grown at 37 °C in Luria-Bertani (LB) Broth [5 g/L yeast extract (Himedia, India); 10 g/L tryptone (Difco, USA); 10 g/L NaCl (PanReac AppliChem, Spain); 100 μg/mL ampicillin (Amresco, USA)] for 16 h under orbital agitation at 200 rpm (Agitorb 200 IC, Norconcessus, Portugal).

3.2 Cloning

The plasmids used in this study are listed in Supplementary Material (Table 7.1).

For the construction of integrative recombinant vectors, DNA from p426_pphIAPP and p426_phIAPP was double digested with *Sac*I (New England Biolabs, USA) and *Kpn*I (New England Biolabs), resolved in 1% agarose gel [agarose electrophoresis grade (Invitrogen life technologies, UK), 40 mM Tris base; 20 mM Acetic acid; 1 mM EDTA (TAE); 5 μg/mL Ethidium bromide (Sigma Aldrich, USA)] and purified with Gel DNA Recovery Kit (Zymoclean Research, USA). The purified DNA was then cloned into the *Sac*I/*Kpn*I restriction sites of pRS304 and pRS306 vectors. The ligation reaction was performed using 2.5 ng/μL of vector and 7.5 ng/μL of insert, according to manufacturer´s instructions (Thermo Scientific, USA). The reactions were incubated for 1 h at 22ºC, followed by 16 h at 16ºC, after which they were used for bacterial transformation.

3.3 Preparation of competent *Escherichia coli* and transformation

Competent cells were prepared as previously described[89]. For the transformation, DNA (30 ng of plasmid DNA or 5 μL of the ligation reaction) was added to competent *E. coli* suspension and incubated on ice for 30 min, followed by a heat-shock at 42ºC for 45 s. After 1 min incubation in ice, cells were ressuspended in 800 μL of SOC [5 g/L yeast extract; 20 g/L tryptone; 5 M NaCl; 1 M KCl (Merck, Germany); 1 M $MgCl_2$ (Merck, Germany); 1 M $MgSO_4$ (Merck, Germany); 1 M glucose (Sigma-Aldrich, USA)] and incubated for 1 h at 37ºC, with orbital agitation at 200 rpm. Cells were pelleted by centrifugation for 1 min at 6000 g and plated onto LB agar media supplemented with ampicillin (100 μg/mL). After incubation overnight at 37ºC, single colonies were inoculated in 2 mL liquid LB/ampicillin media for plasmid DNA extraction.

3.3.1 DNA extraction

The kit ZR Plasmid Miniprep-Classic (Zymo Research, USA) was used to purify plasmid DNA. Briefly, cells suspensions were centrifuged for 1 min at 14000 g and the resulting pellets were resuspended in 200 μL of P1 Buffer. 200 μL of P2 buffer was mixed to the cells suspensions by inverting the tubes 2-4 times to promote the complete cell lysis. Neutralization of the samples was performed by adding 400 μL of P3 buffer. The samples were centrifuged for 3 min at 14000 g and the supernatant was transferred to a Zymo-Spin™ llN column attached to a collection tube, followed by centrifugation for 30 s at 14000 g. The DNA in the column was washed twice by adding 200 μL of Endo-Wash Buffer and 200 μL of Plasmid wash, followed by a centrifugation step. The Zymo-Spin™ llN column was transferred to an Eppendorf and 50 μL of DNA elution buffer were added to the column, followed by a centrifugation for 1 min at 14000 g. Plasmid DNA was stored at -20ºC. Analytical agarose gels were used to monitor the *Sac*I/*Kpn*I restriction patterns of plasmid DNA. The GeneRuler 1 kb DNA Ladder (Thermo Scientific, USA) was used as a molecular weight marker. The identity of novel recombinant clones was checked by DNA sequencing analysis.

3.4 Yeast strains and growth conditions

The *Saccharomyces cerevisiae* strain W303-1A (MATa *can1-100 his3-11,15 leu2-3,112 trp1-1 ura3-1 ade2-1*) was used in all the experiments (Table 7.2, supplementary material). It was grown in YPD medium [10 g/L yeast extract; 20 g/L peptone (Himedia, India); 20 g/L glucose]. The selection of cells encoding plasmids was done in Synthetic Defined (SD) dropout media lacking specific amino acids [0.77 g/L Complete Supplement Mixture-Uracil (CSM-Ura) (MP biomedicals, USA) or CSM-6AA (MP biomedicals, USA) plus the required amino acids; 0.67 g/L Yeast Nitrogen Base (YNB) (Difco, USA); 1% (w/v) raffinose (Sigma-Aldrich, China)]. For all experiments, a pre-inoculum was prepared by inoculating one singly colony from agar plates in 3 mL of SD-raffinose and cells were grown overnight at 30ºC under orbital agitation at 200 rpm. The optical density (OD) at 600 nm (OD_{600}) of cultures was measured (Plate spectrophotometer Power Wave XS, Biotek) and cultures were diluted in fresh SD-raffinose medium to obtain a culture with a final OD_{600} = 0.2 ± 0.02 after 16 h, according to the equation:

$$ODi \times Vi = \frac{ODf}{2^{t/gt}} \times Vf \qquad \textbf{Equation 3.1}$$

Where ODi = initial optical density of the culture, Vi = initial volume of culture, ODf = final optical density of the culture, t = time (16 h), gt = generation time of the strain, Vf = final volume of culture. OD_{600} readings were performed in the plate spectrophotometer Power Wave XS (Biotek).

3.4.1 Yeast transformation

Yeast was incubated in YPD medium overnight at 30ºC under orbital agitation at 200 rpm and diluted to obtain a culture to a final OD_{600} of 0.1 ± 0.01. Cell cultures were incubated for 3.5 h, centrifuged (1500 g for 5 min) and cells were washed with sterile H_2O. The supernatant was discarded, the pellet was resuspended in 1 mL of TE/LiAc [Tris 0.1 M (Carl Roth, Germany); EDTA 10 mM (VWR, Belgium); 100 mM Lithium acetate (Sigma-Aldrich, USA)] and cells suspensions were centrifuged at 6000 g. The competent cells were ressuspended in TE/LiAc. The transformation mixture was prepared as follows: 5 µL of denaturated DNA from salmon sperm (10 µg/µL) (Sigma-Aldrich, USA); 1-2 µL of plasmid DNA; 50 µL of competent cells, 300 µL of PEG/TE/LiAc [40% polyethylene glycol (PEG); TE/LiAc]. Integrative plasmids were linearized with *Pst*I (New England BioLabs, USA) enzyme before yeast transformation.

Cells suspensions were first incubated for 30 min at 30ºC and then for 20 min at 42ºC. Cells were washed with water, pelleted by centrifugation and plated onto SD-Uracil (Ura), SD-Tryptophan (Trp) or SD-Ura-Trp agar. Plates were incubated for 48 h at 30ºC.

3.4.2 Phenotypic assays

For the phenotypic growth assays, cells were grown in SD-raffinose medium to OD_{600} nm 0.1 ± 0.01 and the OD_{600} nm was adjusted to 0.05 ± 0.005. Serial dilutions were performed with a ratio of 1:3, and 5 µl of each dilution was spotted onto solid medium containing glucose [0.77 g/L CSM-Ura or CSM-6AA; 0.67 g/L YNB; standard concentrations of the appropriates amino acids; and 2% (w/v) glucose] or galactose [0.77 g/L CSM-Ura or CSM-6AA; 0.67 g/L YNB; standard concentrations of the appropriates amino acids and 2% (w/v) galactose (Sigma®, Germany)] as the sole carbon sources. Protein expression was regulated by the yeast *GAL1* promoter, allowing tight repression by glucose and ready activation in the presence of galactose[88].Growth was recorded after 48 h incubation at 30°C. Images were acquired using ChemidocTM XRS and Quantity-one® software.

3.4.3 Growth curves

Cell cultures pre-grown in raffinose medium were diluted to OD_{600} 0.03 ± 0.003 in medium containing glucose or galactose. The cultures, 3 biological samples and 3 technical replicates, in a total of 9 replicates, were then incubated at 30°C with shaking for 24 h in a spectrophotometer microplate reader (PowerWave XS Biotek) and cellular growth was monitored hourly by measuring OD_{600}. The data was analyzed using the R studio software. The R package grofit[90] was used to adjust a model-based. The selected models were the Gompertz model, the Gompertz exponential model and the Richards model established by Akaike information criterion (AIC). The growth parameters were estimated from the best model fit. The best model fit and corresponding points were represented graphically. The lag phase, the maximum cell growth, the cell doubling time at maximum growth and the area under curve (AUC) were estimated and represented as 95% confidence intervals**.**

3.4.4 Fluorescence microscopy

Fluorescence microscopy was used to monitor IAPP subcellular dynamics. Cell cultures, obtained as indicated above, were centrifuged at 2000 g for 5 min and ressuspended in SD-galactose to induce IAPP expression. Cells were incubated for 6 h at 30°C and 500 µL of cell suspension were collected by centrifugation at 2000 g for 2.5 min. Cell pellets were washed with 500 µL of phosphate-buffered saline (PBS) and centrifuged at the same conditions. Slides were prepared using 4 µL of cell suspensions and were visualized using a fluorescence microscope (Leica DM6B widefield fluorescence microscope equipped with a Leica Application Suitex software version 1.90.13747 with a cooled CCD camera, Roper Scientific Coolsnap HQ). Images were analyzed using Fiji-ImageJ1.51j8, USA.

3.4.5 Protein Extraction

After 6 h induction of IAPP expression in SD-galactose medium, the OD_{600} of cell suspensions were measured and a normalized number of cells were collected by centrifugation for 4 min at 2500 g. Total protein extracts were obtained using the TCA (trichloroacetic acid) extraction method[91]. Cell pellets were incubated for 20 min with TCA (Sigma-Aldrich, USA) and after centrifugation for 3 min at 15000 g, they were washed with acetone (Fluka Biochemika, USA). The pellets were ressuspended in 200 µL of MURB buffer [50mM sodium phosphate (Fluka Biochemika, Germany); 25mM MES (Sigma-Aldrich, USA); 1% Sodium dodecyl sulfate (SDS) (Merck, Germany); 3 M urea (Carl Roth, Germany); 0,5% β-mercaptoethanol (Sigma-Aldrich, Germany); 1 mM sodium azide (Carl Roth, Germany); proteases and phosphatases inhibitors]. Cells were lysed by 3 cycles of vortexing and incubation on ice. Samples were incubated at 70ºC for 10 min and supernatant was collected by centrifugation for 1 min at 10000 g. Protein extracts were stored at -80ºC or resolved on a SDS-PAGE gel.

3.5 Protein Quantification

A calibration curve was performed using bovine serum albumin (BSA) serial dilutions, ranging from 1 mg/mL to 0.125 mg/mL. 2 µL of each BSA dilution or the protein samples were transferred to a microplate. 100 µL of Bradford Reagent (Bio-Rad, USA) was mixed to the plate and incubated for 10-15 min in the dark. Three technical replicates were done for each sample.

Absorbance was measured at 595 nm and a calibration curve was plotted. The curve was checked for linearity and the concentration of the protein samples were estimated using the calibration curve.

3.6 SDS-PAGE and Immunoblotting

Samples were loaded on 10% SDS gels [30% Acrylamide mix, (Carl Roth, Germany); 1.5 M tris.HCl; 0.5 M tris HCl; 10% SDS; 10%, ammonium persulfate (APS) (G-Biosciences, USA); tetramethylethylenediamine (TEMED) (Merck, Germany)] and transferred to polyvinylidene fluoride (PVDF) membranes (Bio-Rad, USA) using a trans-blot turbo transfer system (Bio-Rad, USA) for 7 min at 25 V. The membranes were boiled for 5 min in PBS to expose the epitopes and improve protein signals[92]. Ponceau S [0, 2% (w/v) Ponceau S (Merck, Germany); 3 %(w/v) TCA; 3% (w/v) sulfosalicylic acid (Merck, Germany)] staining was performed as a control of the transference procedure. The membranes were immersed in the Ponceau S solution for 5 min and washed with bi-distillated water to reveal the presence of the protein bands. The membranes were blocked for 1 h in TBS-T milk [5% skimmed milk (Nestlé, Portugal) prepared in TBS containing 0.01% (v/v) tween20 (Sigma-Aldrich, USA)] (TBS-T) at room temperature, followed by overnight incubation at 4ºC with the primary antibody diluted in TBS-T. The antibodies used are listed in Table 3.1. The membranes were washed 3 times with TBS-T and incubated for 2 h with horseradish peroxidase-conjugated secondary antibodies. The signals were detected using Enhanced Chemiluminescence Prime Western blotting detection reagent (GE Healthcare) in the Chemidoc Equipment XRS (Bio-Rad).

Table 3.1. Antibodies used in this study.

Primary Antibody (1:1000)	Target	Source	Secondary Antibody (1:5000)	Source
Rabbit Sera A133	Human IAPP (residues 20-29)	Kindly provided by Gunilla Westermark[24]	Goat anti-rabbit	Pierce, USA
Anti-GFP	GFP amino acids 1-238	Santa Cruz Biotechnology, USA	Anti-mouse	
Mouse Monoclonal Antibody Anti-Pgk1	Yeast Pgk1 (3-Phosphoglyceric Phosphokinase)	Life Technologies, USA		

3.7 Plasma samples

Plasma samples were collect at APDP (*Associação Protectora de Diabéticos de Portugal*) in EDTA tubes (BD), centrifuged at 3500 rpm for 10 min and stored at -80ºC in aliquots of 200 µL. Total protein content was quantified by the Bradford method and 100 µg, 25 µg and 15 µg of total protein was dissolved in TBS and Protein Sample Buffer [0.24 M Tris; 18% β-Mercaptoetanol (Sigma-Aldrich, USA); 8% SDS; 40% Glycerol (Sigma-Aldrich, Germany); 0.1% Bromophenol Blue, pH 6.8). The samples were heated for 10 min at 45ºC and resolved in a SDS-PAGE gel[93]. Immunoblotting was performed as indicated above.

4. Results

4.1 Optimization of humanized yeast models of IAPP aggregation

One of the main advantages of working with *S. cerevisiae* as a model organism is the availability of a wide selection of vectors that can be used for various purposes. Usually, they are shuttle vectors that can be amplified in bacteria and expressed in yeast, making them useful tools for gene cloning and molecular biology approaches[94].

In yeast, shuttle vectors are maintained either extrachromosomally or by integration into the genome. The centromeric and multi-copy vectors replicate autonomously from CEN and 2µ replication origin sequences, respectively. The transformation process is usually very efficient, resulting in 10^4 - 10^5 transformants per µg of DNA. 2µ-driven plasmids can be found at 20-50 copies per cell. Though, these plasmids are unstable being lost at a frequency of 0.2-2% per generation[95].

Yeast integrative plasmids lack autonomous replication functions in yeast being its replication associated with chromosome duplication during cell division. They are useful to integrate or disrupt genes in the yeast genome by homologous recombination. The frequency of integration is very low (1-10 transformants per µg of DNA). Nevertheless, the transformation frequency can be increased 10-1000 fold following plasmid linearization with restriction enzymes[95]. Integrated DNA sequences are usually very stable, but can be lost at a frequency of approximately 0.1-2% per generation[95]. For the selection of recombinant cells, the yeast vectors encode auxotrophic marker genes, which complement the corresponding mutation in the host yeast genome and restore a given biosynthetic pathway[96].

hIAPP overexpression has been pointed as a risk factor for intracellular aggregation[74,97,98]. Thus, the study of hIAPP proteotoxicity was first addressed in the host laboratory by the cloning of the cDNA corresponding to the unprocessed and mature hIAPP fused to GFP into the multi-copy yeast vector pRS426 (Menezes *et al.*, unpublished)(Figure 4.1).

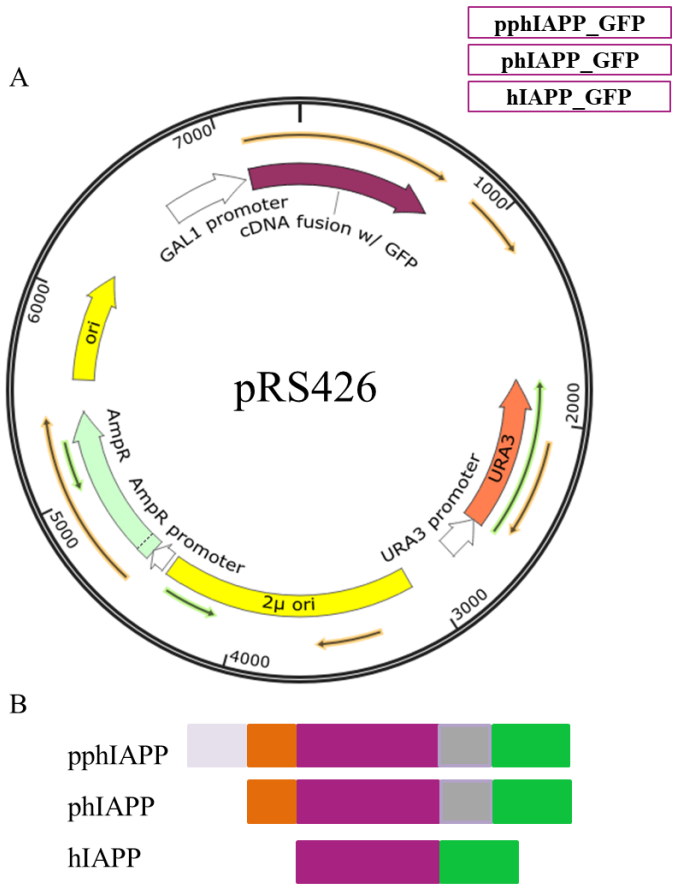

Figure 4.1 Schematic representation of the constructions to express hIAPP in yeast. A) Diagram of the pRS426 vector designed by the SnapGene software (GSL Biotech; available at snapgene.com) with the indication of *GAL1* promoter (white) driven the expression of pphIAPP, phIAPP and hIAPP cDNA fusions with GFP (purple) and the main features of the vector. B) Schematic representation of pphIAPP, phIAPP and hIAPP with the indication of processed amino acid sequences (grey and orange) and the GFP tag (green). Ori – replication origin; AmpR – ampicillin resistance gene (encoding for β-lactamase); GFP – green fluorescent protein; pphIAPP – prepro human IAPP; phIAPP – pro human IAPP; hIAPP – human IAPP.

Data obtained using these models indicated that overexpression of hIAPP in yeast leads to aggregation and cytotoxicity (Menezes *et al*., unpublished), recapitulating the main features of IAPP toxicity in β-cells. In addition, unprocessed hIAPP forms were shown to be slightly more toxic than the mature one (Menezes *et al.* unpublished), in accordance with the notion that inefficient hIAPP processing may be associated with β-cell cytotoxicity. Although the humanized yeast models of IAPP aggregation are very promising, they presented some limitations. The instability inherent to multi-copy vectors, particularly regarding the expression of unprocessed hIAPP forms, led to difficulties in the interpretation of results.

To overcome this limitation, it was decided to integrate the same constructions, as indicated in Figure 4.1 B, into the yeast genome. The construction of novel hIAPP recombinant strains took into consideration two important aspects: (a) the *locus* of integration can affect the strength of expression[93,99] and (b) the expression of a single copy of hIAPP constructions could not be enough to promote aggregation and cytotoxicity, as described for α-synuclein[86].To address these issues, two integrative plasmids, driven integration into the *TRP1* (pRS304) and the *URA3* (pRS306) *loci* and restoring tryptophan and uracil prototrophy respectively, were used (Figure 7.1 supplementary material). The inserts carrying the pphIAPP-GFP and phIAPP-GFP sequences were obtained from the respective pRS426 constructions (Table **7**.1 supplementary material) by digestion with *Sac*I/*Kpn*I and after agarose gel purification they were ligated into pRS304 and pRS306 previously digested with the same enzymes (Table **7**.1 supplementary material). The ligation reactions were transformed in competent *E. coli* and after DNA purification the positive clones were first selected by restriction analysis (Figure 7.2, supplementary material) and their identities were checked by DNA sequencing analysis. The hIAPP-GFP constructions were previously done using the same cloning strategy (Menezes *et al.*, unpublished).

4.1.1 Cytotoxicity of IAPP upon integration into the yeast genome

The use of galactose inducible *GAL1* promoter in yeast allows tight regulation of gene expression according to the carbon source used in culture medium[100,101]. In the presence of glucose, *GAL1* is repressed due to a mechanism called catabolic repression[100]. Raffinose alleviates the effect of catabolic repression but gene expression only starts when cells are faced to galactose conditions. Two sets of strains, prototrophic for tryptophan and uracil, were tested. Each set encodes the mature (hIAPP) and two independent clones of each unprocessed hIAPP form (pphIAPP_Trp_1, pphIAPP_Trp_2, pphIAPP_Ura_1, pphIAPP_Ura_2, phIAPP_Trp_1, phIAPP_Trp_2, phIAPP_Ura_1 and phIAPP_Ura_2) under the control of the *GAL1* promoter, or the empty vector (E). The strains were serially diluted and plated onto repressing (Glu) or inducing (Gal) media for phenotypic growth assays (Figure 4.2). As expected, all strains exhibited a growth similar to the respective control strain (E) in glucose medium. The only exception was pphIAPP_Ura_1, whose growth seems to be impaired for reasons unrelated to pphIAPP expression. Under galactose conditions, all recombinant strains of the Trp set showed a slight growth impairment in comparison with the respective control strain whereas the phIAPP_Ura_1 was the strain of the Ura set exhibiting reduced growth. These results are in agreement with those obtained with the multi-copy plasmids (Menezes *et al*., unpublished), however the cytotoxicity levels were shown to be lower when the constructs are integrated in the genome. The clones pphIAPP_Trp_2; phIAPP_Trp_1, pphIAPP_Ura_2 and phIAPP_Ura_2 were selected for further analysis (Table 7.2 supplementary material).

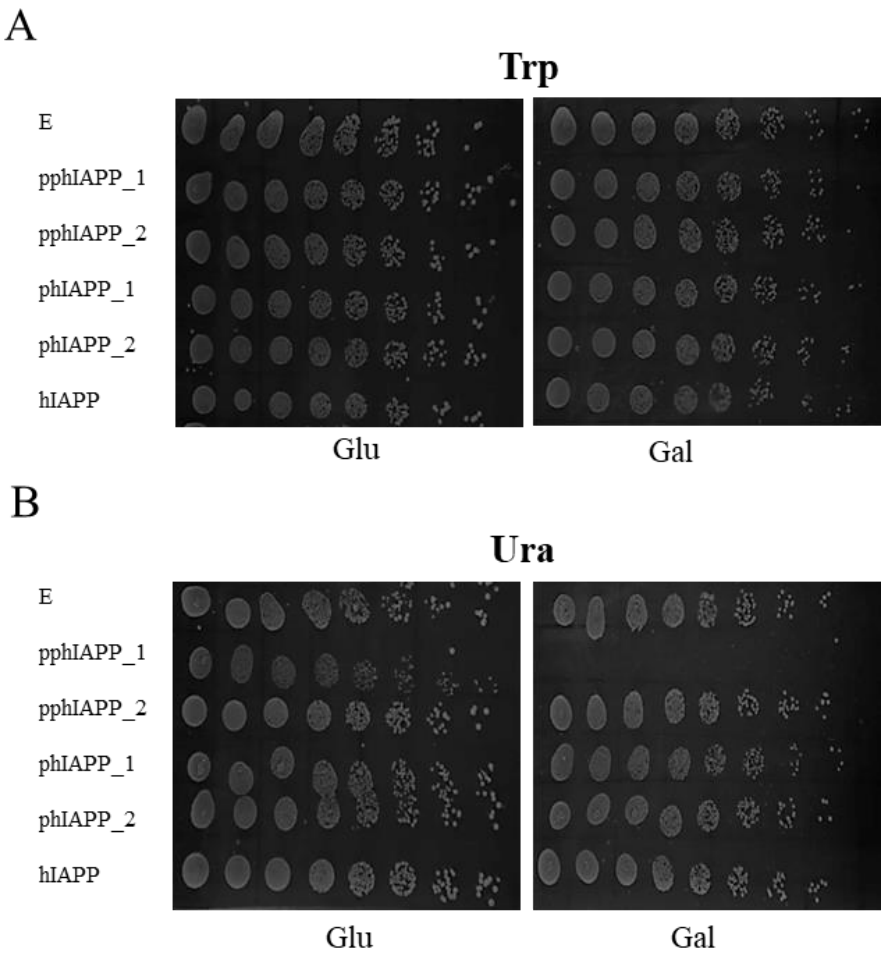

Figure 4.2 Phenotypic growth assays. A) Clones of the Trp set. B) Clones of Ura set. The strains were grown in raffinose medium, serial dilutions were performed with a ratio of 1:3, and 5 µl of each dilution was spotted onto solid medium containing glucose (Glu) – repressing media – or galactose (Gal) – inducing media. Images were recorded after two days incubation at 30ºC. Trp – Tryptophan; Ura – Uracil; E – Empty vector; pphIAPP - prepro human IAPP; pIAPP – pro human IAPP; hIAPP – human IAPP.

As a more refined measurement of cellular growth, the selected strains were subjected to growth curve analysis to evaluate growth parameters potentially affected by the expression of hIAPP. A normalized number of cells were inoculated in galactose medium and cellular growth was monitored hourly for 24 h. The results depicted in Figure 4.3 A-C indicate that growth of all strains from the Trp set was slightly compromised in comparison with the control strain (E). The lag time, which reflects the time required for a cell population to duplicate after the inoculum, is the parameter mostly affected upon pphIAPP and phIAPP expression (Figure 4.3 D-F). Despite the overlap of confidence intervals, there was a tendency for the mean of the recombinant strains to be higher than the mean of the controls. Expression of hIAPP affected majorly the final biomass of the cultures, the lag time and the area under the curve (AUC) in comparison with the respective control strain (Figure 4.3 D-F).

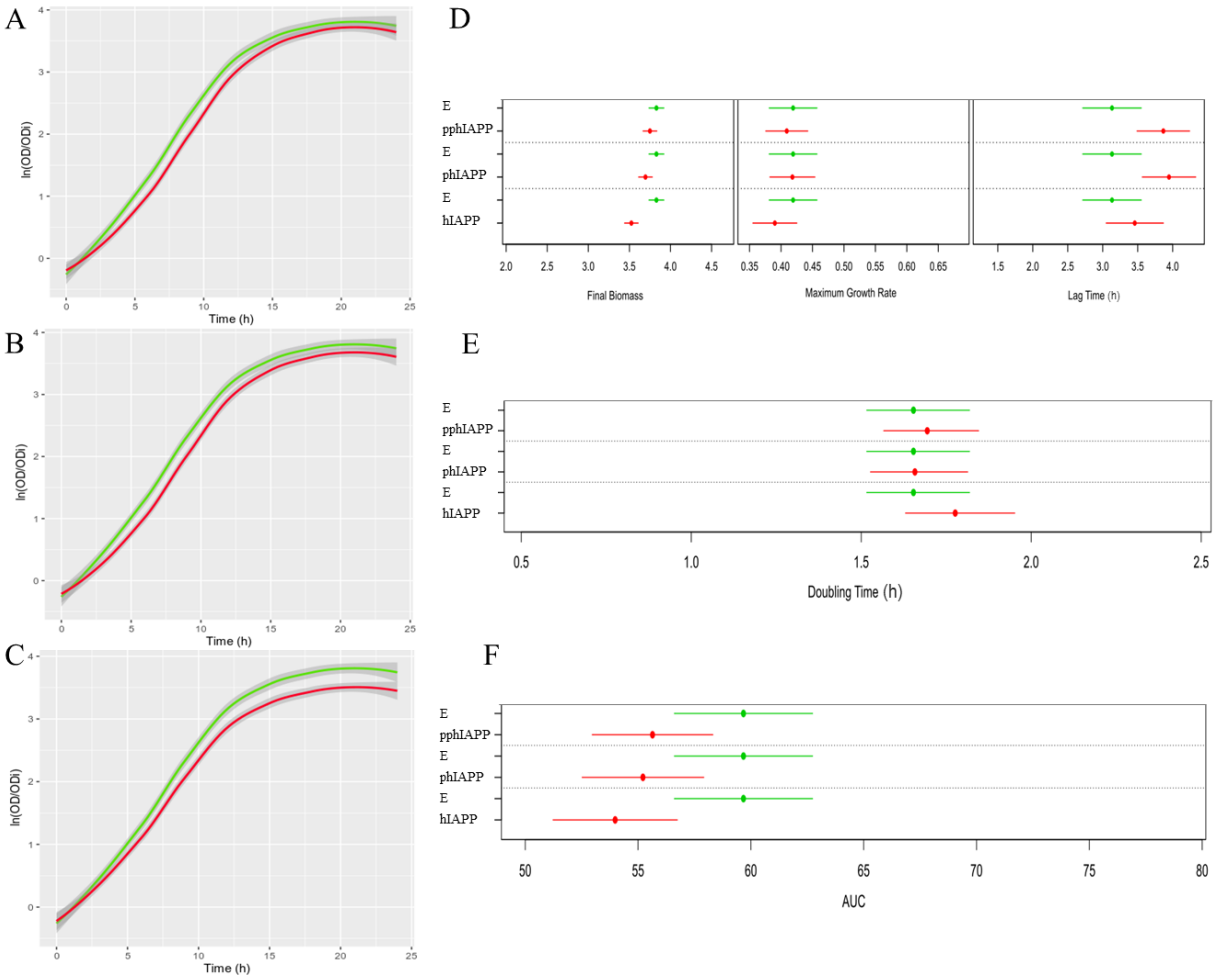

Figure 4.3 Growth curves of strains of the Trp set. Growth was kinetically monitored by OD600 measures and results are expressed as mean values from three independent biological replicates. Growth curves and growth parameters of the humanized strains (red) and the respective controls (green), obtained using an R script are represented. (A) pphIAPP model, (B) phIAPP model (C) hIAPP model. Graphical representation of the confidence intervals with 95% of confidence for (D) the final biomass, maximum growth rate and lag time, (E) doubling time and (F) AUC. Trp – Tryptophan; E – Empty vector; pphIAPP - prepro human IAPP; pIAPP – pro human IAPP; hIAPP – human IAPP; AUC – area under the curve.

The strains from the Ura set were also subjected to growth curve analysis. The growth of pphIAPP was slightly affected in comparison with the control strain (E) whereas phIAPP remained unaltered. Among all strains, the growth of the hIAPP model was the most drastically affected (Figure 4.4 A-C). The final biomass and AUC of the model expressing hIAPP were the parameters showing the highest differences as compared to the control condition (Figure 4.4 D-F). The maximum growth rate and doubling time were also affected. Despite the overlap of confidence intervals, there was a tendency for the increase of the doubling time and reduction of the maximum growth rate.

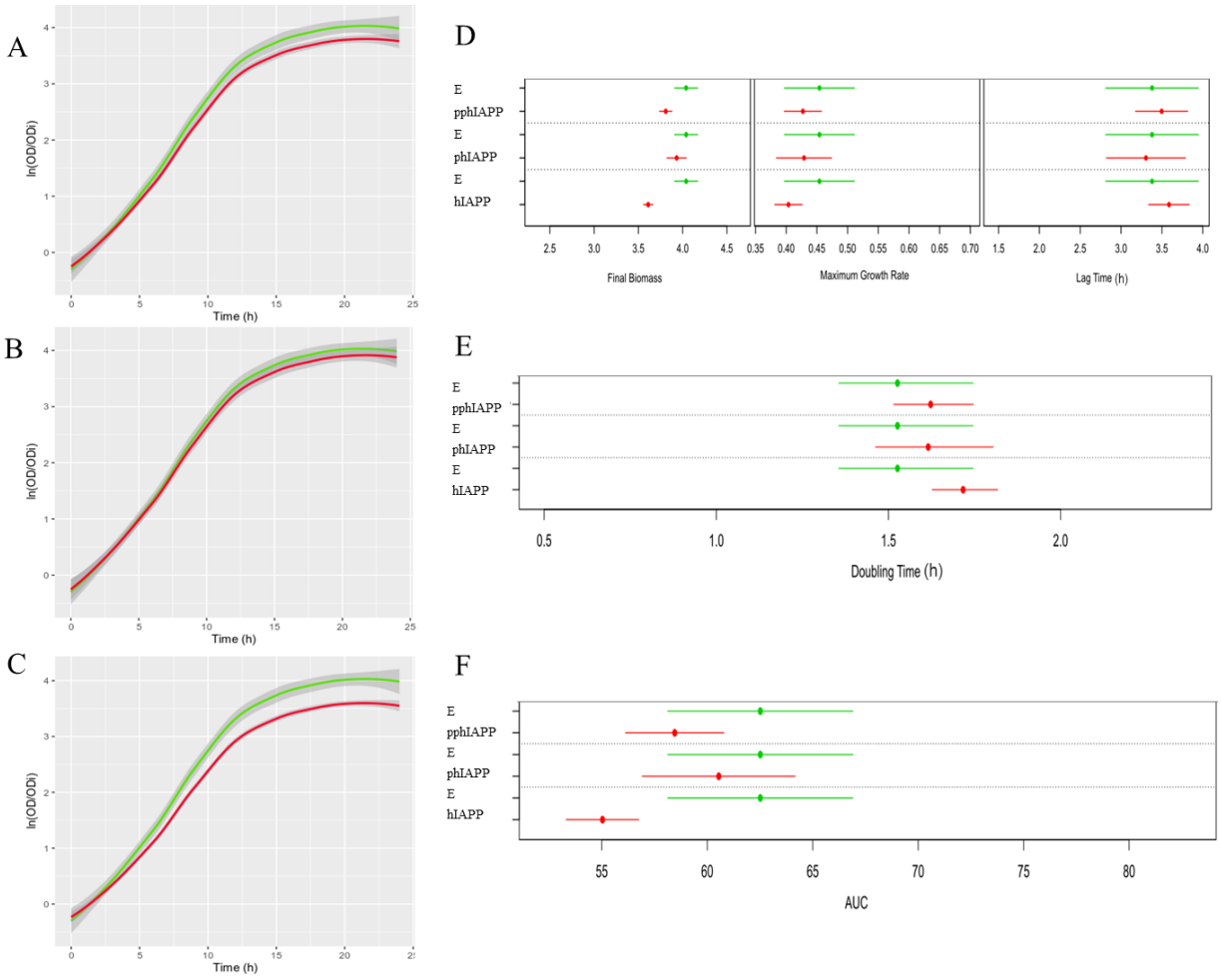

Figure 4.4 Growth curves of strains of the Ura set. Growth was kinetically monitored by OD_{600} measures and results are expressed as mean values from three independent biological replicates. Growth curves and growth parameters of the humanized strains (red) and the respective controls (green), obtained using an R script are represented. (A) pphIAPP model, (B) phIAPP model (C) hIAPP model. Graphical representation of the confidence intervals with 95% of confidence for (D) the final biomass, maximum growth Rate and lag Time, (E) doubling time and (F) AUC. Ura – uracil; E – Empty vector; pphIAPP - prepro human IAPP; pIAPP – pro human IAPP; hIAPP – human IAPP; AUC – area under the curve.

In general terms, it can be suggested that hIAPP expression in the strains of Trp set seem to confer a higher degree of toxicity in comparison with the strains of the Ura set. Notwithstanding, hIAPP cytotoxicity observed in these strains is too low and should be improved to increase the robustness of the models.

4.1.2 Subcellular localization of hIAPP

hIAPP subcellular localization was monitored by fluorescence microscopy. As shown in Figure 4.5, similar results were obtained for both the Trp and Ura set of strains. phIAPP and hIAPP were shown to be dispersed throughout the cytosol and in a cellular compartment resembling the nucleus. However, staining with specific nuclei probes such as 4',6-Diamidine-2'-phenylindole dihydrochloride (DAPI) is required to confirm this issue. No evident hIAPP aggregates could be detected under these conditions (Figure 4.5). Another feature that seems to be associated with hIAPP expression is the presence of large vacuoles. Previous unpublished data from the host laboratory suggests that this phenomenon can be associated with a cellular stress[102], in this case mediated by hIAPP expression.

Unexpectedly, the fluorescence of cells expressing pphIAPP was shown to be almost undetectable, as shown in supplementary material Figure 7.3 A. A possible explanation for this result is the instability of the fusion protein in yeast and/or the removal of the GFP tag after processing of the COOH-terminal region of pphIAPP. This issue will be discussed in more details in the next sections.

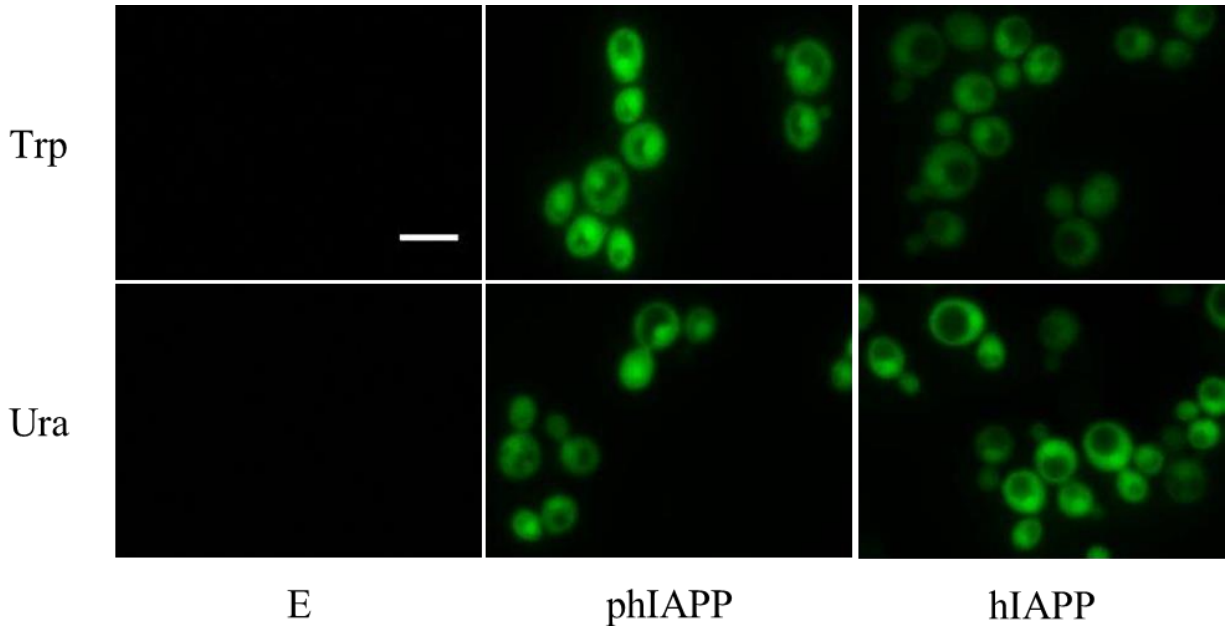

Figure 4.5 Fluorescence microscopy of yeast cells expressing phIAPP and hIAPP. Cells were first grown in raffinose media and IAPP expression was induced with galactose for 6 h. Scale bar= 10 μm. Trp – tryptophan; Ura – uracil; E – Empty vector; phIAPP – pro human IAPP; hIAPP – human IAPP.

4.2 Generation of humanized yeast models encoding two integrated copies of hIAPP

The previous results had demonstrated a very low level of cytotoxicity when a single copy of the constructions were integrated in the yeast genome, in agreement to what was described for α-synuclein[86]. Therefore, in an effort to increase the robustness of the models a second copy of the respective constructions were integrated in the yeast genome. For that, pphIAPP_Trp_2 cells were transformed with pphIAPP_Ura_2 DNA to generate the strain pphIAPP_Trp-Ura (Table 7.2 supplementary material) encoding two copies of the pphIAPP DNA. A similar approach was used for the generation of the double transformed phIAPP strain (Table 7.2 supplementary material), using the phIAPP_Trp_1 cells and the DNA of phIAPP_Ura_2. The double-transformed hIAPP strain, expressing the mature form, was previously generated using a similar strategy (Menezes *et al*., unpublished).

4.2.1 Cytotoxicity of the optimized hIAPP models

To evaluate the impact of hIAPP expression in the optimized models, the strains were first grown in raffinose medium and were then serially diluted and plated on repression (Glu) or inducing (Gal) media for phenotypic growth assays (Figure 4.6). Integrating a second copy of the constructions in the yeast genome potentially increases the intracellular accumulation of the respective proteins thus exacerbating their toxic functions. Indeed, the growth of the phIAPP_Trp-Ura model was shown to be more dramatically affected in relation to the control strain (Figure 4.6) than the equivalent strains encoding one copy of the hIAPP cDNA (Figure 4.2). Otherwise, the phenotypic growth assays did not show any significant growth impairment of the pphIAPP and the hIAPP strains.

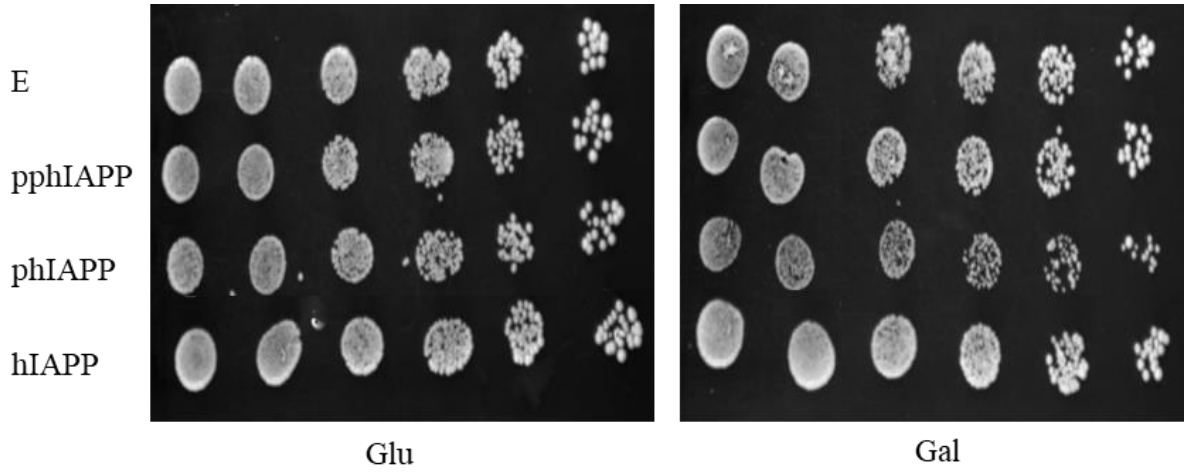

Figure 4.6 Phenotypic growth assays of the humanized yeast models expressing two copies of pphIAPP, phIAPP and hIAPP. The strains were grown in raffinose medium, serial dilutions were performed with a ratio of 1:3, and 5 µl of each dilution was spotted onto solid medium containing glucose (Glu) – repressing media – or galactose (Gal) – inducing media. Images were recorded after two days incubation at 30ºC. E – Empty vector; pphIAPP - prepro human IAPP; pIAPP – pro human IAPP; hIAPP – human IAPP.

In order to investigate in greater detail the cellular growth of these strains, they were subjected to growth curve analysis. A normalized number of cells were inoculated in galactose medium and cellular growth was monitored hourly for 24 h. The results in Figure 4.7 A-C show that the growth profile of pphIAPP strain is similar to that of the control strain, in agreement with results of the phenotypic growth assays. A clear impairment of phIAPP_Trp-Ura strain growth was observed as compared to the control strain (Figure 4.7 A-C), also consistent with the results of the phenotypic growth assays. In particular, the growth parameters of final biomass, maximum growth rate, and doubling time, were shown to be significantly altered, impacting on the AUC of the growth curves (Figure 4.7 C-F).

The only parameter that seems to be only negatively affected by the expression of hIAPP in the optimized strain is the final biomass (Figure 4.7 A), although there was a tendency towards the increase of the doubling time and a reduction in the maximum growth rate as compared to the control strain (Figure 4.7 C-E). The fact that phIAPP expression impairs growth in greater extent than hIAPP supports the notion that unprocessed forms are potentially more toxic than the mature hIAPP form. The growth of the pphIAPP_Trp-Ura model was similar to the control strain suggesting that pphIAPP expression did not compromise cellular growth.

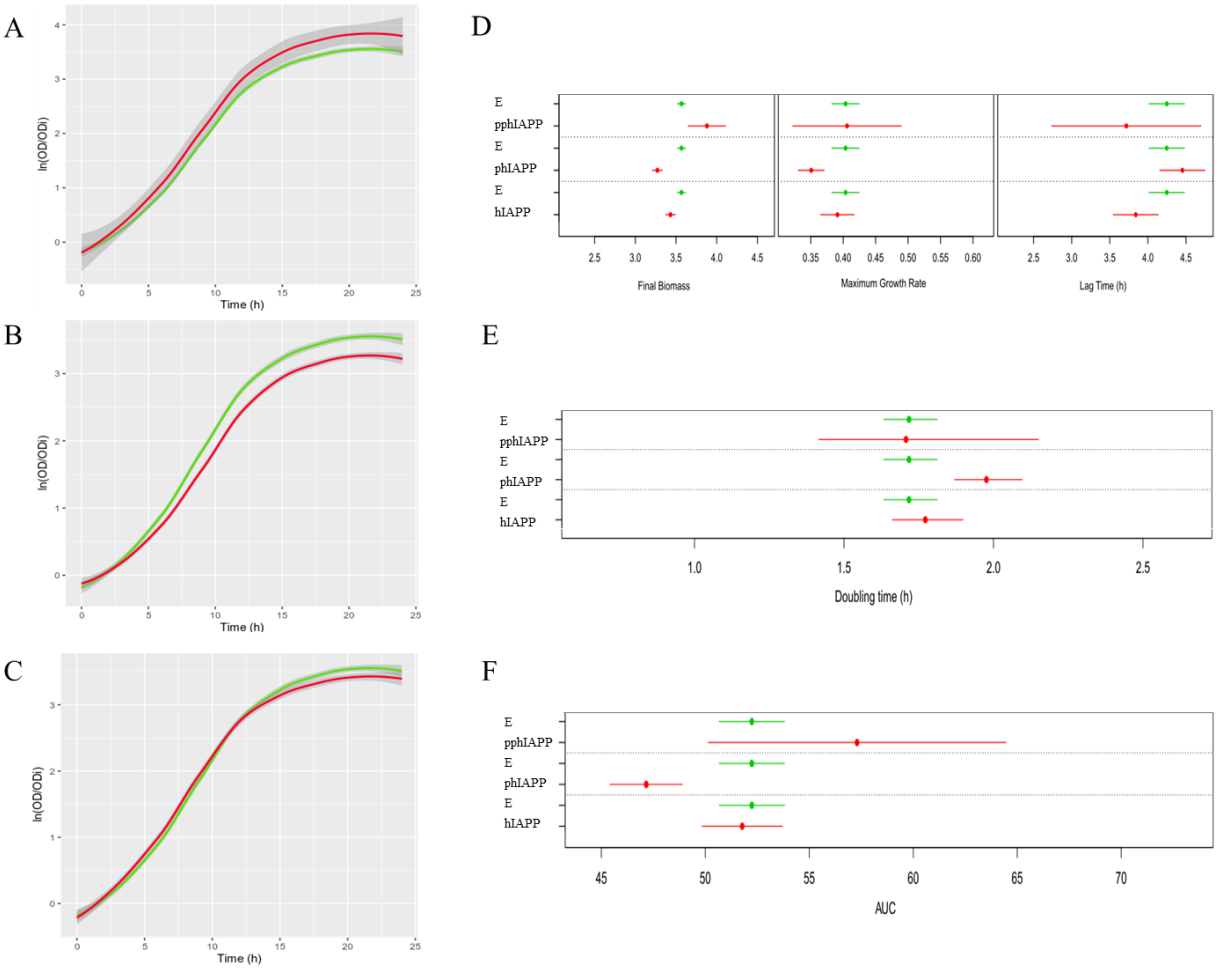

Figure 4.7 Growth curves of the optimized hIAPP models. Growth was kinetically monitored by OD600 measures and results are expressed as mean values from three independent biological replicates. Growth curves and growth parameters of the humanized strains (red) and the respective controls (green), obtained using a R script are represented. (A) pphIAPP model (B) phIAPP model (C) hIAPP model. Graphical representation of the confidence intervals with 95% of confidence for (D) the final biomass, maximum growth rate and lag time, (E) doubling time and (F) AUC. Ura – uracil; E – Empty vector; pIAPP – pro human IAPP; hIAPP – human IAPP; AUC – area under the curve.

4.2.2 Subcellular localization of IAPP and unprocessed forms in the humanized model expressing two copies of each construction

To investigate hIAPP subcellular localization in the optimized models, protein expression was induced in galactose media for 6 h. As observed in the model expressing one copy of hIAPP, GFP fluorescence in the optimized strain was dispersed throughout the cytoplasm and obvious aggregates could not be detected (Figure 4.8). Remarkably, the strain expressing two copies of phIAPP displayed punctate structures that seem to accumulate in the lumen of the vacuoles and in association with the vacuole membrane (Figure 4.8). Co-localization studies using vacuole probes are required to clarify this issue. The fluorescence of cells expressing pphIAPP was shown to be residual, as shown in supplementary material Figure 7.3 B.

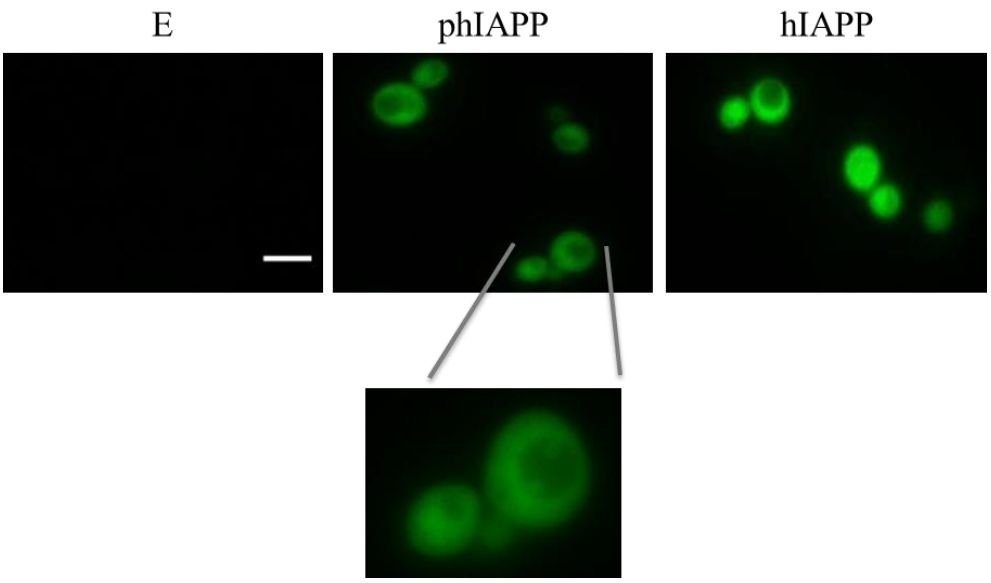

Figure 4.8 Fluorescence microscopy of hIAPP and phIAPP optimized yeast models. Cells were first grown in raffinose media and IAPP expression was induced with galactose for 6 h. The phIAPP and hIAPP model and an amplification of the punctate structures that seems to accumulate in cells expressing phIAPP. Scale bar= 10 μm. E – Empty vector; phIAPP – pro human IAPP.

4.3 hIAPP processing in yeast

IAPP is processed by signal-peptidases and convertases to yield mature IAPP and some evidences suggest that unprocessed human IAPP forms are more amyloidogenic than the mature ones. To evaluate hIAPP expression and processing in yeast, strains expressing pphIAPP, phIAPP and hIAPP from multi-copy plasmids and the single- and double-integrated versions, were subjected to immunoblotting analysis using antibodies against an internal sequence (residues 20-29) of hIAPP (A133) and the GFP tag.

For the expression driven by the single copy vectors encoding *TRP1* and *URA3* selectable markers, it was only possible to detect an evident protein signal of phIAPP from the Ura set using the A133 antibody (Figure 4.9 B, upper panel). As an alternative, the membranes were incubated with the anti-GFP antibody, which revealed the presence of specific signals that were absent in the control strain (E) (Figure 4.9, middle panels). Remarkably, extracts of cells expressing pphIAPP and phIAPP displayed a band corresponding to the molecular weight of mature hIAPP fused to GFP (~32 kDa) indicating that endogenous yeast enzymes were able to process hIAPP. It is noteworthy to mention that processing of pphIAPP seems to be more efficient than phIAPP according to the high intensity of protein signal corresponding to intermediate unprocessed forms of phIAPP (~35 kDa) (Figure 4.9 B, middle panel).

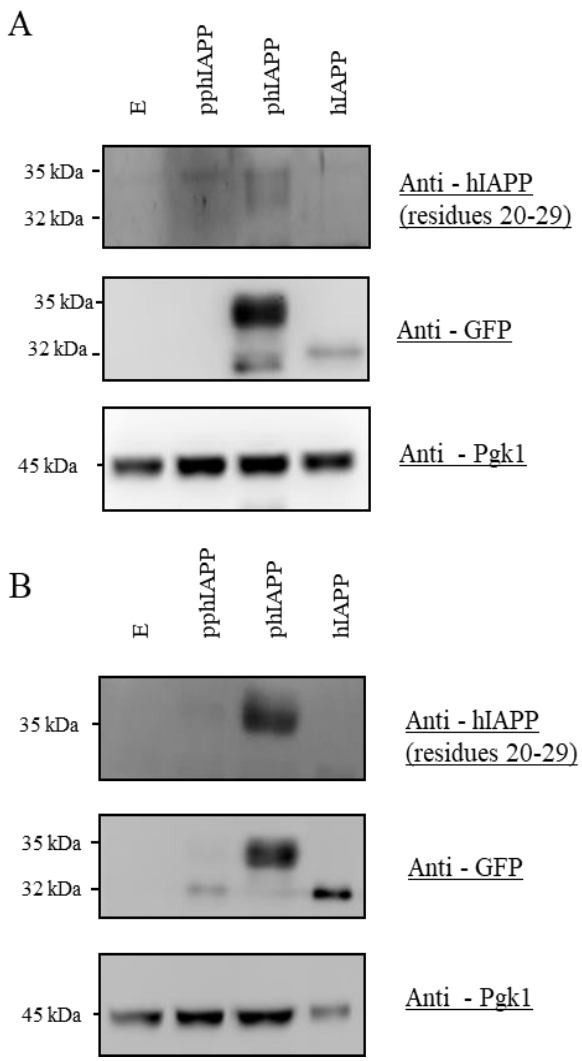

Figure 4.9 IAPP expression and processing in humanized strains encoding a single copy of pphIAPP, phIAPP and hIAPP cDNA. Cells were incubated for 6 h in galactose medium and total proteins were extracted using the TCA method. Immunoblot was performed using the antisera anti-hIAPP (residues 20-29) and anti-GFP antibodies. Pgk1 was used as loading control. (A) Tryptophan set of strains) and (B) Uracil set of strains. E – Empty vector; pphIAPP - prepro human IAPP; phIAPP – pro human IAPP; hIAPP – human IAPP; pgk1 - 3-phosphoglycerate kinase; GFP – green fluorescent protein; TCA - trichloroacetic acid.

Aiming to improve the detection of different hIAPP forms, the whole procedure was repeated using the strains encoding the double-integrated hIAPP constructions. As depicted in Figure 4.10, the protein signals provided by the use of the A133 antibody were highly improved. The membranes were also incubated with the anti-GFP antibody, which revealed the presence of strong protein signals. The strain expressing a double-integrated pphIAPP construction exhibited a signal whose molecular weight is lower than mature hIAPP fused to GFP (~32 kDa), which may correspond to the pphIAPP processed COOH-terminus fused to GFP (Figure 4.1 B). This result corroborates the previous ones showing that endogenous yeast enzymes efficiently process hIAPP. In addition, Figure 4.10 further supports that pphIAPP processing is more efficient than phIAPP.

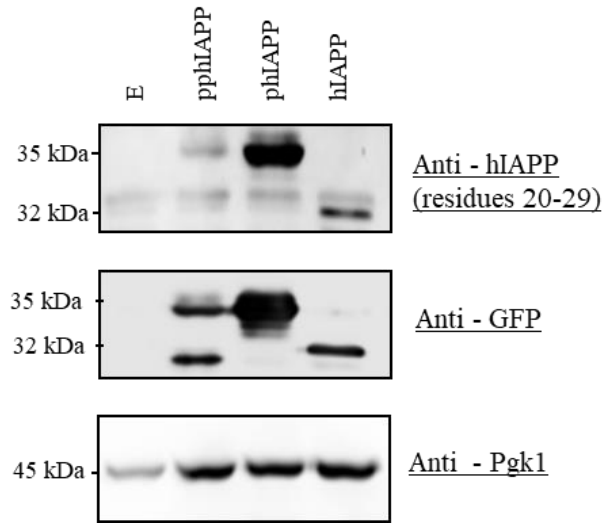

Figure 4.10 IAPP expression and processing in humanized strains encoding double-integrated versions of pphIAPP, phIAPP and hIAPP cDNA. Cells were incubated for 6 h in galactose medium and total proteins were extracted using the TCA method. Immunoblot was performed using the antisera anti-hIAPP (residues 20-29) and anti-GFP antibodies. Pgk1 was used as loading control. E – Empty vector; pphIAPP - prepro human IAPP; pIAPP – pro human IAPP; hIAPP – human IAPP; pgk1 - 3-phosphoglycerate kinase; GFP – green fluorescent protein.

hIAPP expression and processing patterns were also investigated in the strains encoding the cDNA for pphIAPP, phIAPP and hIAPP from multi-copy vectors. The protein signals provided by the use of the A133 antibody were further improved in comparison with the double-integrated strain, being possible to detect a faint signal corresponding to a phIAPP form with increased electrophoretic mobility that could not be detected in other conditions (Figure 4.11 A, upper panel). Incubation of the membranes with the anti-GFP antibody revealed the presence of several processing intermediates that were undetectable using the other constructions (Figure 4.11 B, upper panel). Although the high frequency of plasmid loss associated with the expression driven by multi-copy vectors were shown to be a limitation for the growth assays, these results suggest that expressing driven by multi-copy vectors represents a powerful tool to address hIAPP processing in yeast.

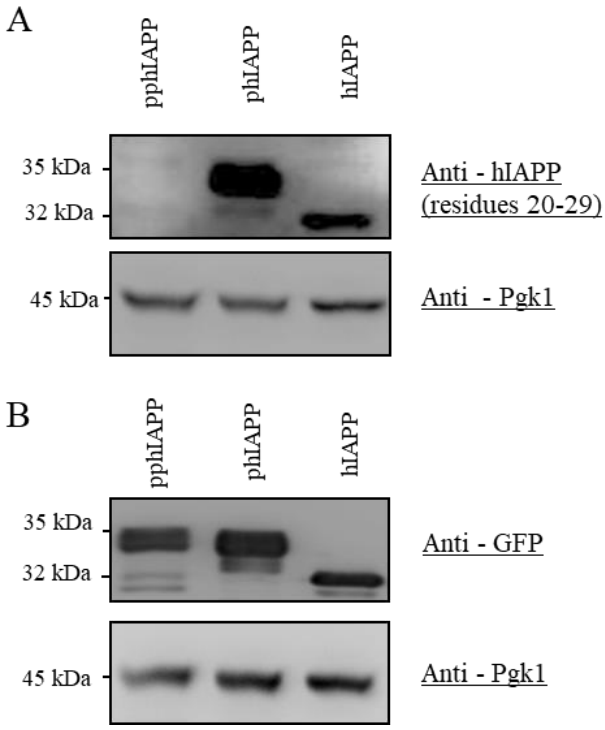

Figure 4.11 IAPP expression and processing in humanized strains encoding pphIAPP, phIAPP and hIAPP cDNA from multi-copy vectors. Cells were incubated for 6 h in galactose medium and total proteins were extracted using the TCA method. Immunoblot was performed using A) the antisera anti-hIAPP (residues 20-29) and B) anti-GFP antibodies. Pgk 1was used as loading control. E – Empty vector; pphIAPP - prepro human IAPP; pIAPP – pro human IAPP; hIAPP – human IAPP; pgk1 - 3-phosphoglycerate kinase; GFP – green fluorescent protein.

4.4 Detection of human IAPP oligomers in plasma samples

The next goal was to evaluate the presence of hIAPP oligomers in the plasma as potential indicators of diabetes. For that, the blood samples of five volunteers were collected. After obtaining the plasma samples, they were processed as described by Jackson *et al*.[69]. This study reported that IAPP expressed in pancreas of T2DM and Alzheimer's or dementia patients accumulates in the brain and precipitates as independent plaques or co-precipitates with amyloid β, meaning that the oligomers that reach the brain are most probably synthesized in the pancreas, circulate in the bloodstream and may accumulate in various organs.

Immunoblotting from SDS gels loaded with 100 μg of total plasma proteins revealed the presence of several bands in all the samples, mostly probably representing the unspecific recognition of high abundant plasma proteins such as albumin and immunoglobulins (Figure 4.12 A), which may mask the specific signal of hIAPP oligomers. To overcome this technical limitation, the gels were loaded with 25 μg of total plasma proteins. Remarkably, under this condition it was possible to detect a signal of a molecular weight of 22-24 kDa only in the plasma sample of the volunteer diagnosed with LADA (Latent Autoimmune Diabetes in Adults) (sample 4), which could correspond to hIAPP oligomers (Figure 4.12 B). Noteworthy, the hIAPP signal detected in the immunoblotting analysis seems to be specific as it was detected in protein extracts from yeast cells expressing the pphIAPP-GFP fusion. It was further tested the whether hIAPP signals could be detected using lower amounts (15 μg) of total plasma proteins. For this purpose, only sample 4 (S4) and sample 2 (S2) were loaded in the gel but hIAPP signals were show to be absent. As shown in Figure 4.12 C, it was possible to corroborate the presence of the 22 kDa signal, which appears very intense in S4, but was also present as a faint signal in sample 2. The decrease of protein concentration completely abolished detection of hIAPP.

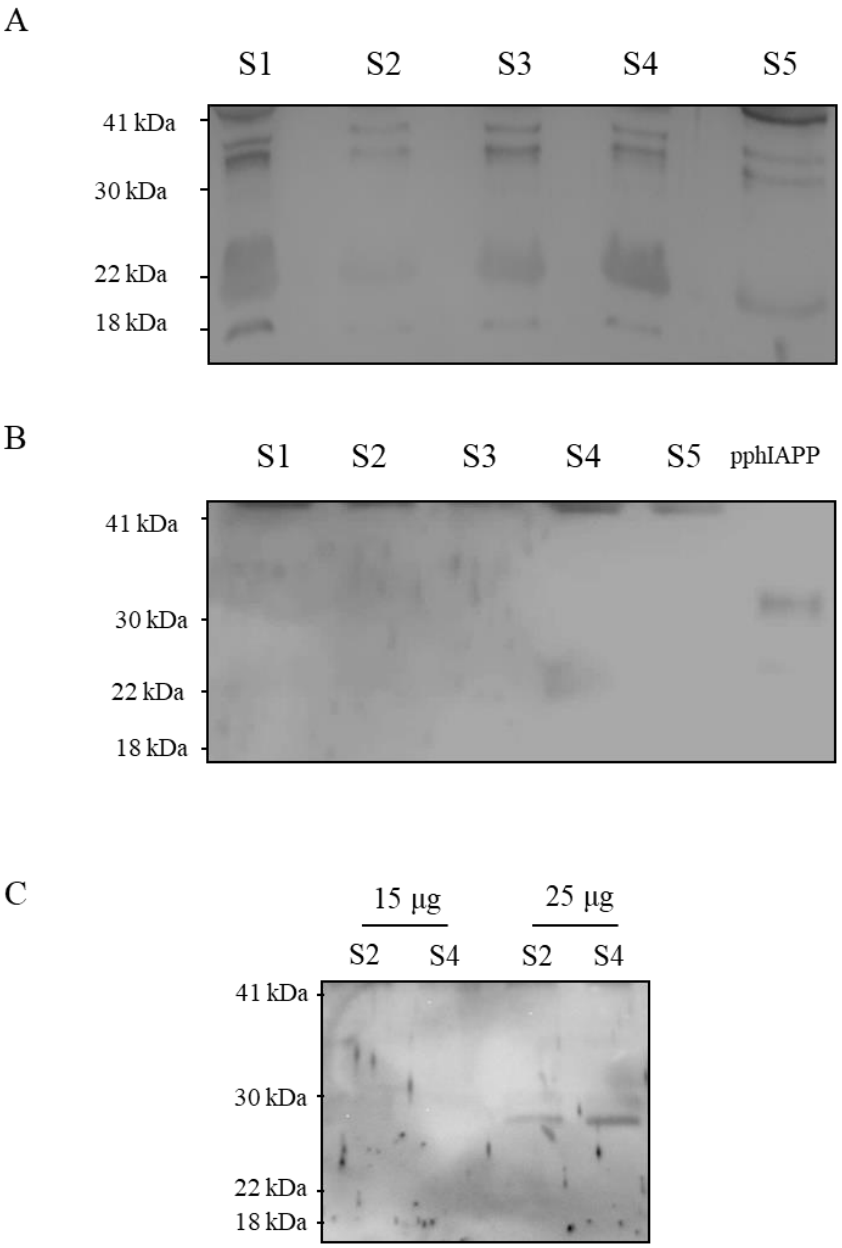

Figure 4.12 Detection of IAPP in plasma samples. A) 100 µg of total plasma proteins were loaded on SDS gels and IAPP was detected using the rabbit sera A133, which recognizes the hIAPP 20-29 epitope. B) The SDS gels were loaded with 25 µg of total plasma proteins. Protein extracts obtained from yeast cells expressing ppIAPP-GFP were used as controls. C) The SDS gels were loaded with 15 or 25 µg of total plasma proteins of S2 and S4. S1 - sample 1; S2 - sample 2; S3 - sample 3; S4 - sample 4; S5 - sample 5; pphIAPP_GFP – prepro human IAPP; GFP – green fluorescent protein.

5. Discussion

5.1 Novel yeast models of hIAPP proteotoxicity

The cytotoxic role of hIAPP oligomers and amyloid deposition in the islets have a significant impact in the pathology of DM[8]. An important question that remains to be answered is whether formation of islet amyloids is a pathogenic mechanism contributing to the development of T2DM or a consequence of the islet malfunctioning. It was observed that islet amyloid was detectable in a baboon colony before the development of T2DM and the amount of islet amyloid is correlated with the progression of the disease[103]. Based on that, it was proposed that the combination of a predisposing genetic background with environmental factors such as obesity and high-fat diets can lead to insulin resistance and overstimulation of β-cells to secrete insulin. As a consequence there is also the concomitant overexpression of IAPP favoring its intra- and extracellular accumulation. However, the mechanism underlying IAPP aggregation and deposition remain to be elucidated[103]. Therefore, a simple experimental model as yeast can be a valuable tool to dissect the intracellular events of IAPP oligomerization and to reveal the hallmarks of hIAPP fibril formation.

Yeast models encoding the cDNA for mature and unprocessed hIAPP forms from multi-copy vectors were previously used in the host laboratory to study the cellular effects of hIAPP overexpression and aggregation. Given the artifacts associated with the use of these expression systems, mostly due the high frequency of loss (0.2-2% per generation)[95], novel strains were designed. They were constructed by integrating the cDNA for pphIAPP, phIAPP or hIAPP into the yeast genome, in the *TRP1* and *URA3 loci*. So, two sets of strains, prototrophic for tryptophan and uracil (Table 7.2 supplementary material), were generated.

The first experiments addressed the growth of strains expressing pphIAPP, phIAPP and hIAPP by phenotypic assays. The recombinant strains of the Trp set showed slight growth impairment (Figure 4.2) whereas the phIAPP clones of the Ura set were the only marginally affected by the expression of the respective protein. To complement these data, the 24-hour growth curves of strains were compared. The results were in accordance with the phenotypic assays and the recombinant strains of the Trp set were shown to be slightly affected by the expression of mature and unprocessed hIAPP forms (Figure 4.3 A-C). The expression of pphIAPP and phIAPP seems to increase the lag phase of the cultures in comparison with the control (Figure 4.3 D), which represents the time required for a cell population to duplicate after the inoculum. This indicates that the expression of the protein somehow interferes with cell metabolism, delaying cell growth that is then recovered after cells are able to adapt to the stress conditions induced by hIAPP expression. The final biomass is the parameter mostly affected by the expression of hIAPP (Figure 4.3 D), which seems to be a consequence of alterations of the maximum growth rate and consequently the doubling time of the cultures (Figure 4.3 D, E). These results corroborate the previous results showing impaired cell growth of the hIAPP strain. The growth of pphIAPP and particularly hIAPP strains with integrations in the *URA3 locus* (Ura set) were also compromised relatively to the control strain (Figure 4.4 A). Taken together, the data suggest that integration of one copy of hIAPP constructs affects negatively the growth of strains from both the Trp and Ura set.

The subcellular localization of the protein fusions, monitored by fluorescence microscopy, indicates that both phIAPP and hIAPP from the Trp and Ura set of strains (Figure 4.5) presented a cytosolic distribution with no visible aggregates. These results indicate that these models cannot recapitulate the intracellular aggregates observed in β-cells, as it was observed for the expression of phIAPP driven by multi-copy vectors (Menezes *et al.*, unpublished). An interesting finding of these experiments was the presence of large vacuoles in the cells encoding the phIAPP and hIAPP cDNA. Data from the host laboratory suggests that this phenomenon can be associated with cellular stress[102], in this case mediated by hIAPP expression. Surprisingly, the fluorescence of cells expressing pphIAPP

was shown to be almost undetectable (Figure 7.3 A supplementary material). The possible explanation for this result is the removal of the GFP tag after processing of the COOH-terminal region of pphIAPP, which was further confirmed by the immunoblotting experiments (Figure 4.9-Figure 4.11).

In an attempt to increase the robustness of the models, a second copy of the cDNA for pphIAPP and phIAPP were integrated into the yeast genome and the resulting strains were tested together with a previously constructed strain expressing two copies of hIAPP. The cell growth of hIAPP model was not significantly impaired by the integration of a second copy of the corresponding cDNA. The most impaired parameter was the final biomass (Figure 4.7 D-F) suggesting that the two copies of the protein slightly affect strains growth and replication. The cell growth of the pphIAPP strain did not show any significant difference relatively to the control strain (Figure 4.7). Indeed, pphIAPP protein levels seem to be strongly affected as indicated by the immunoblotting (Figure 4.10) and microscopy assays (Figure 7.3 B supplementary material). The GFP signal of strains encoding two copies of pphIAPP are higher than those observed in the equivalent strains expressing pphIAPP from *TRP1* or *URA3* integrative constructions (Figure 7.3 B supplementary material). However, it is still residual compared to the strains expressing phIAPP and hIAPP, which further suggests the instability of pphIAPP transcripts and/or pphIAPP protein degradation as a cellular defense mechanism. Quantitative real time PCR and protein stability assays should be performed to elucidate this question. The low fluorescence signals of pphIAPP strains (Figure 7.3 supplementary material) seems to be also a consequence of pphIAPP processing by the convertases to yield mature IAPP, leading to the removal of COOH-terminal region of the peptide fused with the GFP tag. This hypothesis is confirmed by the presence of several hIAPP processing intermediates (Figure 4.9-Figure 4.11) observed in the immunoblotting assays, particularly the one whose molecular weight is lower that of the hIAPP (Figure 4.10, compare lanes 2 and 4 in the middle panel; Figure 4.11 B, compare lanes 1 and 3 in the upper panel). In humans, the prohormone convertases PC2 and PC1/3 process the COOH and the NH_2 terminal of phIAPP at the dibasic amino acid residues (lysine and arginine). The candidate enzyme exerting this function is the homologous yeast Kex2[104], a Ca^{2+}-dependent serine protease involved in proprotein processing[105]. Like the human counterparts, Kex2 also cleaves dibasic sites in target peptides and belongs to the family of subtilisin-like proteases. The evolutionary conservation of proprotein convertase function between yeast and mammals allows the use of yeast to investigate aberrant phIAPP processing, which can help understanding the impact of phIAPP processing on intracellular oligomerization and islet amyloid formation.

Interestingly, the strain carrying two copies of the cDNA for phIAPP was the only one displaying pronounced growth defects (Figure 4.6 and Figure 4.7). In addition, this strain exhibits punctate structures resembling protein aggregates that seem to be located in the vacuole (Figure 4.8). The data suggest that cells try to cope with phIAPP toxicity (Figure 4.6) by sequestering it into the vacuoles. Although co-localization studies are required to clarify this issue, it can be speculated that increased expression of phIAPP, by the insertion of an additional copy of the phIAPP cDNA into the yeast genome, induces proteotoxic stress and cells try to get rid of these toxic species by sequestering them into the vacuole. The presence of phIAPP processing intermediates in islet amyloids of T2DM patients was already demonstrated and it was also suggested that an increase in phIAPP levels may also contribute to islet amyloid deposition[49]. In agreement with these notions, the data discussed above demonstrate that overexpression of phIAPP driven by two integrated copies of phIAPP cDNA promotes cellular stress; furthermore it leads to IAPP aggregation and impairs cellular growth thereby validating these model as a valuable tool to investigate the molecular mechanisms underlying phIAPP aggregation and proteotoxicity.

To conclude, the expression of mature and unprocessed hIAPP forms driven by single genome integrations in the *TRP1* and *URA3 loci* triggers growth impairment and cellular stress. Since immunoblotting procedures were performed simultaneously for the extracts from cells expressing the

TRP1 and *URA3* constructs, and using a normalized number of cells, it is plausible to conclude that expression driven by the *URA3* construct is more efficient than the *TRP1* construct (Figure 4.9). However, the negative impact caused by a single copy of cDNA of pphIAPP, phIAPP and hIAPP expression in these strains is lower compared to those driven by the multi-copy constructs (Menezes *et al.*, unpublished).

Notwithstanding, the integration of a second copy of the respective cDNAs, particularly encoding for phIAPP can promote aggregation and cytotoxicity as described for the α-synuclein[86].

5.2 hIAPP oligomers indicators of diabetes

A methodology for detecting the presence of IAPP oligomers in human plasma samples was optimized aiming at the evaluation of these species as early indicators of diabetes. For that, the plasma samples of healthy volunteers and a patient diagnosed with LADA were subjected to immunoblotting analysis using an antibody against hIAPP residues 20-29. The results indicate the presence of a very promising protein signal of 22-24 kDa (Figure 4.12), possible corresponding to IAPP oligomers. A further procedure to validate these results is the utilization of antibodies recognizing oligomeric structures, such as the A11[106]. It is reported that A11 efficiently recognizes intracellular oligomeric IAPP species in the β-cells of hIAPP transgenic mice[98] and in the human pancreatic tissue ofT2DM patients[98,107]. These antibodies are useful to identify small IAPP oligomers *in vitro*; however their use in biological materials and tissue sections can be lead to artifacts since specificity could be compromised by the cross-reaction with a variety of molecules with β-conformation[108].

Analysis of human plasma samples for protein studies can be a complex task due to the presence of a high concentration of albumin and immunoglobulins. Indeed, this was shown to be a limitation in this study leading to the unspecific protein signals in the immunoblotting analysis (Figure 4.12 A). Removal of these proteins is an approach often used to study low abundancy proteins such as hIAPP or hIAPP oligomers. There are a plenty of techniques to deplete proteins from plasma but one easy way to do it is using depletion columns kits. Samples are loaded in a pre-filled convenient disposable column and can be quickly processed. This could be a suitable alternative, although it can lead to the partial loss of proteins of interest. Another alternative is the use of DynaBeads derivatized with anti-hIAPP antibodies to remove albumin, immunoglobulins and other molecules that may interfere with specific signals. In order to follow this methodology it is necessary to guarantee that the assemblages of IAPP are not discarded along with the other proteins.

In conclusion, the presence of IAPP oligomers in the blood remains to be elucidated and the literature regarding the subject is also scarce. An important immediate goal to pursue is the development of a simpler approach aimed at detecting these molecules and using them as a potential biomarker of islet amyloid and also as a new target for new therapies.

6. References

1. WHO. *Definition, Diagnosis and Classification of Diabetes Mellitus*. (1999). doi:WHO/NCD/NCS/99.2
2. American Diabetes Association (ADA). Standard of medical care in diabetes - 2017. *Diabetes Care* **40 (sup 1),** s4–s128 (2017).
3. Gepts, W. Pathologic anatomy of the pancreas in juvenile diabetes mellitus. *Diabetes* **14,** 619–633 (1965).
4. Maclean, N. & Ogilvie, R. F. Quantitative estimation of the pancreas islet tissue in diabetic subjects. *Diabetes* **4,** 367–376 (1955).
5. Zimmet, P. The burden of type 2 diabetes: are we doing enough? *Diabetes Metab.* **29,** 6S9-6S18 (2003).
6. Soto, C. Unfolding the role of protein misfolding in neurodegenerative diseases. *Nat. Rev. Neurosci.* **4,** 49–60 (2003).
7. Stefani, M. Protein misfolding and aggregation: New examples in medicine and biology of the dark side of the protein world. *Biochim. Biophys. Acta - Mol. Basis Dis.* **1739,** 5–25 (2004).
8. Jurgens, C. A. *et al.* B-Cell Loss and B-Cell Apoptosis in Human Type 2 Diabetes Are Related To Islet Amyloid Deposition. *Am. J. Pathol.* **178,** 2632–40 (2011).
9. Hartl, F. U. Protein Misfolding Diseases. *Annu. Rev. Biochem.* **86,** 28.1-28.6 (2017).
10. Westermark, P. Quantitative studies on amyloid in the islets of Langerhans. *Ups. J. Med. Sci.* **77,** 91–4 (1972).
11. Westermark, P., Wernstedt, C., Wilander, E. & Sletten, K. A novel peptide in the calcitonin gene related peptide family as an amyloid fibril protein in the endocrine pancreas. *Biochem. Biophys. Res. Commun.* **140,** 827–831 (1986).
12. Cooper, G. J. *et al.* Purification and characterization of a peptide from amyloid-rich pancreases of type 2 diabetic patients. *Proc. Natl. Acad. Sci. U. S. A.* **84,** 8628–32 (1987).
13. Hull, R. L., Westermark, G. T., Westermark, P. & Kahn, S. E. Islet amyloid: A critical entity in the pathogenesis of type 2 diabetes. *J. Clin. Endocrinol. Metab.* **89,** 3629–3643 (2004).
14. Haataja, L., Gurlo, T., Huang, C. J. & Butler, P. C. Islet amyloid in type 2 diabetes, and the toxic oligomer hypothesis. *Endocr. Rev.* **29,** 303–316 (2008).
15. Roberts, A. N. *et al.* Molecular and functional characterization of amylin, a peptide associated with type 2 diabetes mellitus. *Proc Natl Acad Sci U S A* **86,** 9662–9666 (1989).
16. Ohlsson, H., Karlsson, K. & Edlund, T. IPF1, a homeodomain-containing transactivator of the insulin gene. *EMBO J.* **12,** 4251–9 (1993).
17. Watada, H. *et al.* Involvement of the homeodomain-containing transcription factor PDX-1 in islet amyloid polypeptide gene transcription. *Biochem Biophys Res Commun* **229,** 746–51. (1996).
18. Kahn, S. E. *et al.* Evidence of Cosecretion of Islet Amyloid Polypeptide and Insulin by β-Cells. *Diabetes* **39,** 634–638 (1990).
19. Westermark, P., Wilander, E., Westermark, G. T. & Johnson, K. H. Islet amyloid polypeptide-like immunoreactivity in the islet B cells of Type 2 (non-insulin-dependent) diabetic and non-diabetic individuals. *Diabetologia* **30,** 887–892 (1987).
20. Woods, S. C., Lutz, T. a, Geary, N. & Langhans, W. Pancreatic signals controlling food intake; insulin, glucagon and amylin. *Philos. Trans. R. Soc. Lond. B. Biol. Sci.* **361,** 1219–1235 (2006).
21. Martin, C. The physiology of amylin and insulin: maintaining the balance between glucose secretion and glucose uptake. *Diabetes Educ.* **32,** 101S–104S (2006).
22. Silvestre, R. a *et al.* Selective amylin inhibition of the glucagon response to arginine is extrinsic to the pancreas. *Am. J. Physiol. Endocrinol. Metab.* **280,** E443–E449 (2001).
23. Sanke, T., Bell, G. I., Sample, C., Rubenstein, A. H. & Steiner, D. F. An islet amyloid peptide is derived from an 89-amino acid precursor by proteolytic processing. *J. Biol. Chem.* **263,** 17243–17246 (1988).
24. Paulsson, J. F. & Westermark, G. T. Aberrant Processing of Human Proislet Amyloid Polypeptide Results in Increased Amyloid Formation. *Diabetes* **54,** 2117–2125 (2005).
25. Marzban, L. *et al.* Role of β-Cell Prohormone Convertase (PC)1/3 in Processing of Pro-Islet Amyloid Polypeptide. *Diabeteses* **53,** 141–148 (2004).
26. Wang, J. *et al.* The prohormone convertase enzyme 2 (PC2) is essential for processing pro-islet amyloid polypeptide at the NH2-terminal cleavage site. *Diabetes* **50,** 534–539 (2001).
27. Marzban, L., Soukhatcheva, G. & Verchere, C. B. Role of carboxypeptidase E in processing of pro-islet amyloid polypeptide in β-cells. *Endocrinology* **146,** 1808–1817 (2005).
28. Leckström, A., Björklund, K., Permert, J., Larsson, R. & Westermark, P. Renal elimination of islet amyloid polypeptide. *Biochem. Biophys. Res. Commun.* **239,** 265–8 (1997).
29. Bennett, R. G., Duckworth, W. C. & Hamel, F. G. Degradation of amylin by insulin-degrading enzyme. *J. Biol. Chem.* **275,** 36621–36625 (2000).
30. Guan, H., Chow, K.M, Shan, R., Rhodes, C.J, Hersh, L. . Degradation of Islet Amyloid Polypeptide by

Neprilysin. *Diabetologia* **55,** 2989–2998 (2012).
31. Zraika, S. *et al.* Neprilysin impedes islet amyloid formation by inhibition ofs fibril formation rather than peptide degradation. *J. Biol. Chem.* **285,** 18177–18183 (2010).
32. Westermark, P., Engström, U., Johnson, K., Westermark, G. & Betsholtz, C. Islet amyloid polypeptide: pinpointing amino acid residues linked to amyloid fibril formation. *Proc. Natl. Acad. Sci. U. S. A.* **87,** 5036–40 (1990).
33. Howard, C. F. Insular amyloidosis and diabetes mellitus in Macaca nigra. *Diabetes* **27,** 357–364 (1978).
34. Johnson, K. H., Hayden, D. W., O'Brien, T. D. & Westermark, P. Spontaneous diabetes mellitus-islet amyloid complex in adult cats. *Am. J. Pathol.* **125,** 416–9 (1986).
35. Nilsson, M. R. & Raleigh, D. P. Analysis of amylin cleavage products provides new insights into the amyloidogenic region of human amylin. *J. Mol. Biol.* **294,** 1375–85 (1999).
36. Jaikaran, E. T. *et al.* Identification of a novel human islet amyloid polypeptide beta-sheet domain and factors influencing fibrillogenesis. *J. Mol. Biol.* **308,** 515–25 (2001).
37. Scrocchi, L. A. *et al.* Identification of minimal peptide sequences in the (8-20) domain of human islet amyloid polypeptide involved in fibrillogenesis. *J. Struct. Biol.* **141,** 218–227 (2003).
38. Kajava, A. V., Aebi, U. & Steven, A. C. The parallel superpleated beta-structure as a model for amyloid fibrils of human amylin. *J. Mol. Biol.* **348,** 247–252 (2005).
39. Nanga, R. P. R. *et al.* Three-Dimensional Structure and Orientation of Rat Islet Amyloid Polypeptide Protein in a Membrane Environment by Solution NMR Spectroscopy. *J AM Chem Soc.* **131,** 8252–8261 (2009).
40. Westermark, P., Li, Z. & Westermark, G. Effects of beta cell granule components on human islet amyloid polypeptide fibril formation. *Febs* **379,** 203–206 (1996).
41. Janciauskiene, S., Eriksson, S., Carlemalm, E. & Ahrén, B. B Cell Granule Peptides Affect Human Islet Amyloid Polypeptide (IAPP) Fibril Formationin Vitro. *Biochem. Biophys. Res. Commun.* **236,** 580–585 (1997).
42. Westermark, G. *et al.* Amyloid formation in response to β cell stress occurs in vitro, but not in vivo, in islets of transgenic mice expressing human islet amyloid polypeptide. *Mol Med* **1,** 542–553 (1995).
43. D'Alessio, D. A. *et al.* Pancreatic expression and secretion of human islet amyloid polypeptide in a transgenic mouse. *Diabetes* **43,** 1457–1461 (1993).
44. Bennett, R. G., Hamel, F. G. & Duckworth, W. C. An insulin-degrading enzyme inhibitor decreases amylin degradation, increases amylin-induced cytotoxicity, and increases amyloid formation in insulinoma cell cultures. *Diabetes* **52,** 2315–2320 (2003).
45. Ceriello, A. Oxidative stress and glycemic regulation. *Metabolism.* **49,** 27–29 (2000).
46. Kapurniotu, A. *et al.* Contribution of advanced glycosylation to the amyloidogenicity of islet and amyloid polypeptide. *Eur. J. Biochem.* **251,** 208–216 (1998).
47. W. K. Ward *et al.* Disproportionate elevation of immunoreactive proinsulin in Type 2 (non-insulin-dependent) diabetes mellitus and in experimental insulin resistance. *Diabetologia* **30,** 698–702 (1987).
48. Krampert, M. *et al.* Amyloidogenicity of recombinant human pro-islet amyloid polypeptide (ProIAPP). *Chem. Biol.* **7,** 855–871 (2000).
49. Westermark, G. T., Steiner, D. F., Gebre-Medhin, S., Engström, U. & Westermark, P. Pro Islet Amyloid Polypeptide (ProIAPP) Immunoreactivity in the Islets of Langerhans. *Ups. J. Med. Sci.* **105,** 97–106 (2000).
50. de Koning, E. J. P. *et al.* Human islet amyloid polypeptide (IAPP) accumulates at similar sites in islets of transgenic mice and humans. *Diabetes* **43,** 640–644 (1994).
51. Janson, J., Ashley, R. H., Harrison, D., McIntyre, S. & Butler, P. C. The mechanism of islet amyloid polypeptide toxicity is membrane disruption by intermediate-sized toxic amyloid particles. *Diabetes* **48,** 491–498 (1999).
52. Huang, C. J. *et al.* Calcium-activated calpain-2 is a mediator of beta cell dysfunction and apoptosis in type 2 diabetes. *J. Biol. Chem.* **285,** 339–348 (2010).
53. Li, X. L. *et al.* Involvement of mitochondrial dysfunction in human islet amyloid polypeptide-induced apoptosis in INS-1E pancreatic beta cells: An effect attenuated by phycocyanin. *Int. J. Biochem. Cell Biol.* **43,** 525–534 (2011).
54. Huang, C., Lin, C., Haataja, L. & Gurlo, T. High expression rates of human islet amyloid polypeptide induce endoplasmic reticulum stress–mediated β-cell apoptosis, a characteristic of humans with type 2 but not type 1 diabetes. *Diabetes* **56,** 2016–2027 (2007).
55. Masters, S. L. *et al.* Activation of the Nlrp3 inflammasome by islet amyloid polypeptide provides a mechanism for enhanced IL-1b in type 2 diabetes. *Nat. Immunol.* **11,** 897–904 (2011).
56. Sheedy, F. J. *et al.* CD36 coordinates NLRP3 inflammasome activation by facilitating the intracellular nucleation from soluble to particulate ligands in sterile inflammation. *Nat Immunol.* **14,** 812–820 (2014).
57. Westwell-Roper, C. Y., Ehses, J. A. & Verchere, C. B. Resident macrophages mediate islet amyloid

polypeptide-induced islet IL-1β production and β-cell dysfunction. *Diabetes* **63,** 1698–1711 (2014).
58. Costes, S. *et al.* β-Cell Dysfunctional ERAD/Ubiquitin/Proteasome System in Type 2 Diabetes Mediated by Islet Amyloid Polypeptide–Induced UCH-L1 Deficiency. **60,** 227–238 (2011).
59. Rivera, J. F. *et al.* Human-IAPP disrupts the autophagy/lysosomal pathway in pancreatic β-cells: protective role of p62-positive cytoplasmic inclusions. *Cell Death Differ.* **18,** 415–426 (2011).
60. Halban, P. A. *et al.* β-Cell failure in type 2 diabetes: Postulated mechanisms and prospects for prevention and treatment. *J. Clin. Endocrinol. Metab.* **99,** 1983–1992 (2014).
61. May, P. C., Boggs, L. N. & Fuson, K. S. Neurotoxicity of Human Amylin in Rat Primary Hippocampal Cultures: Similarity to Alzheimer's Disease Amyloid-β Neurotoxicity. *J. Neurochem.* **61,** 2330–2333 (1993).
62. Lorenzo, a, Razzaboni, B., Weir, G. C. & Yankner, B. a. Pancreatic islet cell toxicity of amylin associated with type-2 diabetes mellitus. *Nature* **368,** 756–760 (1994).
63. Hoppener, J. W., Nieuwenhuis, M. ., Vroom, T. M., Ahrén, B. & Lips, C. J. Role of islet amyloid in type 2 diabetes mellitus: Consequence or Cause? *Mol. Cell. Endocrinol.* **197,** 205–212 (2002).
64. Ritzel, R. A. & Butler, P. C. Replication increases β-cell vulnerability to human islet amyloid polypeptide-induced apoptosis. *Diabetes* **52,** 1701–1708 (2003).
65. Udayasankar, J. *et al.* Amyloid formation results in recurrence of hyperglycaemia following transplantation of human IAPP transgenic mouse islets. *Diabetologia* **52,** 145–153 (2009).
66. Paulsson, J. F. *et al.* High plasma levels of islet amyloid polypeptide in young with new-onset of type 1 diabetes mellitus. *PLoS One* **9,** 1–5 (2014).
67. Gong, W. *et al.* Amylin deposition in the kidney of patients with diabetic nephropathy. *Kidney Int.* **72,** 213–218 (2007).
68. S. Despa. K. Margulies, L. Chen, A. Knowlton, P. Havel, H. Taegtmeyer, D. Bers, F. D. Hyperamylinemia contributes to cardiac dysfunction in obesity and diabetes - a study in humans and rats. *Circ Res* **110,** 598–608 (2012).
69. Jackson, K. *et al.* Amylin deposition in the brain: A second amyloid in Alzheimer disease? *Ann. Neurol.* **74,** 517–526 (2013).
70. Despa, F. & DeCarli, C. Amylin: what might be its role in Alzheimer's disease and how could this affect therapy? *Expert Rev Proteomics* **10,** 403–405 (2013).
71. de Koning, E. J., Bodkin, N. L., Hansen, B. C. & Clark, A. Diabetes mellitus in Macaca mulatta monkeys is characterised by islet amyloidosis and reduction in beta-cell population. *Diabetologia* **36,** 378–384 (1993).
72. Ma, Z., Westermark, G. T., Johnson, K. H., O'Brien, T. D. & Westermark, P. Quantitative immunohistochemical analysis of islet amyloid polypeptide (IAPP) in normal, impaired glucose tolerant, and diabetic cats. *Amyloid* **5,** 255–261 (1998).
73. Fox, N. *et al.* Human islet amyloid polypeptide transgenic mice as a model of non-insulin-dependent diabetes mellitus (NIDDM). *FEBS Lett* **323,** 40–44 (1993).
74. Yagui, K., Yamaguchi, T., Kanatsuka, A. & Shimada, F. Formation of islet amyloid fibrils in beta-secretory granules of transgenic mice expressing human islet amyloid polypeptide/amylin. *Eur. J.* (1995).
75. Verchere, C. B. *et al.* Islet amyloid formation associated with hyperglycemia in transgenic mice with pancreatic beta cell expression of human islet amyloid polypeptide. *Proc. Natl. Acad. Sci. U. S. A.* **93,** 3492–6 (1996).
76. Soeller, W. C. *et al.* Islet amyloid-associated diabetes in obese Avy/a mice expressing human islet amyloid polypeptide. *Diabetes* **47,** 743–750 (1998).
77. O'Brien, T. D., Butler, P. C., Kreutter, D. K., Kane, L. A. & Eberhardt, N. L. Human islet amyloid polypeptide expression in COS-1 cells: a model of intracellular amyloidogenesis. *Am. J. Pathol.* **147,** 609–616 (1995).
78. Sidoli, F. R., Mantalaris, A. & Asprey, S. P. Modelling of Mammalian Cells and Cell Culture Processes. *Cytotechnology* **44,** 27–46 (2004).
79. Sherman, F. Getting Started with Yeast. *Methods Enzymol.* **194,** 3–21 (1991).
80. Fruhmann, G. *et al.* Yeast buddies helping to unravel the complexity of neurodegenerative disorders. *Mech. Ageing Dev.* **161,** 288–305 (2017).
81. Botstein, D., Chervitz, S. A. & Cherry, J. M. Yeast as a Model Organism. *Genetics* **277,** 1259–1260 (1997).
82. Foury, F. Human genetic diseases: A cross-talk between man and yeast. *Gene* **195,** 1–10 (1997).
83. Mager, W. H. & Winderickx, J. Yeast as a model for medical and medicinal research. *Trends Pharmacol. Sci.* **26,** 265–273 (2005).
84. Outeiro, T. F. & Muchowski, P. J. Molecular genetics approaches in yeast to study amyloid diseases. *J. Mol. Neurosci.* **23,** 49–59 (2004).

85. Gitler, A. D. Beer and bread to brains and beyond: Can yeast cells teach us about neurodegenerative disease? *NeuroSignals* **16,** 52–62 (2007).
86. Outeiro, T. F. & Lindquist, S. Yeast Cells Provide Insight into Alpha-Synuclein Biology and Pathobiology. *Science (80-.).* **302,** 1772–1775 (2003).
87. Krobitsch, S. & Lindquist, S. Aggregation of huntingtin in yeast varies with the length of the polyglutamine expansion and the expression of chaperone proteins. *Proc. Natl. Acad. Sci. U. S. A.* **97,** 1589–94 (2000).
88. St John, T. P., Scherer, S., McDonell, M. W. & Davis, R. Deletion Analysis of the Saccharomyces GAL Gene Cluster Transcription from Three Promoters. *J. Mol. Biol.* **152,** 317–334 (1981).
89. Inoue, H., Nojima, H. & Okayama, H. High efficiency transformation of Escherichia coli with plasmids. *Gene* **96,** 23–28 (1990).
90. Kahm, M., Hasenbrink, G., Lichtenberg-frate, H., Ludwig, J. & Kschischo, M. Grofit: Fitting biological growth curves. *J. Stat. Softw.* **33,** 1–21 (2010).
91. Miller-Fleming, L., Cheong, H., Antas, P. & Klionsky, D. J. Detection of Saccharomyces cerevisiae Atg13 by western blot. *Autophagy* **10,** 514–517 (2014).
92. Oskarsson, M. E. *et al.* In vivo seeding and cross-seeding of localized amyloidosis: A molecular link between type 2 diabetes and Alzheimer disease. *Am. J. Pathol.* **185,** 834–846 (2015).
93. Karim, A., Curran, K. & Alper, H. Characterization of plasmid burden and copy number in Saccharomyces cerevisiae for optimization of metabolic engineering applications. *FEMS Yeast Res.* **13,** 1–18 (2014).
94. Sikorski, R. S. & Hieter, P. A system of shuttle vectors and yeast host strains designed for efficient manipulation of DNA in Saccharomyces cerevisiae. *Genetics* **122,** 19–27 (1989).
95. Singh, K. K. & Heinemann, J. a. Yeast plasmids. *Methods Mol. Biol.* **62,** 113–130 (1997).
96. Pronk, J. T. Auxotrophic Yeast Strains in Fundamental and Applied Research. *Appl. Environ. Microbiol.* **68,** 2095–2100 (2002).
97. O'Brien, T., Butler, A. E., Roche, P. C., Johnson, K. H. & Butler, P. C. Islet amyloid polypeptide in human insulinomas Evidence for intracellular Amyloidogenesis. *Diabetes* **43,** 329–336 (1994).
98. Gurlo, T. *et al.* Evidence for Proteotoxicity in β Cells in Type 2 Diabetes Toxic Islet Amyloid Polypeptide Oligomers Form Intracellularly in the Secretory Pathway. *Am. J. Pathol.* **176,** 861–869 (2010).
99. Çakar, Z. P., Sauer, U. & Bailey, J. E. Metabolic engineering of yeast: The perils of auxotrophic hosts. *Biotechnol. Lett.* **21,** 611–616 (1999).
100. Johnston, M., Flick, J. S. & Pexton, T. Multiple mechanisms provide rapid and stringent glucose repression of GAL gene expression in Saccharomyces cerevisiae. *Mol. Cell. Biol.* **14,** 3834–3841 (1994).
101. Lohr, D., Venkov, P. & Zlatanova, J. Transcriptional regulation in the yeast GAL gene family: a complex genetic network. *FASEB J.* **9,** 777–787 (1995).
102. Vaz, M. Unraveling phytochemicals with potential therapeutic application for neurogeneneration. (Universidade Nova de Lisboa, 2017).
103. Guardado-Mendoza, R. *et al.* Pancreatic islet amyloidosis, beta-cell apoptosis, and alpha-cell proliferation are determinants of islet remodeling in type-2 diabetic baboons. *Proc. Natl. Acad. Sci. U. S. A.* **106,** 13992–13997 (2009).
104. Brenner, C. Subtleties among subtilases The structural biology of Kex2 and furin-related prohormone convertases. *EMBO Rep.* **4,** 937–938 (2003).
105. Fuller, R. S., Sterne, R. E. & Thorner, J. Enzymes required for yeast prohormone processing. *Annu. Rev. Physiol.* **50,** 345–362 (1988).
106. Kayed, R. *et al.* Fibril specific, conformation dependent antibodies recognize a generic epitope common to amyloid fibrils and fibrillar oligomers that is absent in prefibrillar oligomers. *Mol. Neurodegener.* **2,** 18 (2007).
107. Zhao, H. L. *et al.* Amyloid oligomers in diabetic and nondiabetic human pancreas. *Transl. Res.* **153,** 24–32 (2009).
108. Zraika, S. *et al.* Toxic oligomers and islet beta cell death: guilty by association or convicted by circumstantial evidence? *Diabetologia* **53,** 1046–1056 (2009).
109. Christianson, T. W., Sikorski, R. S., Dante, M., Shero, J. H. & Hieter, P. Multifunctional yeast high-copy-number shuttle vectors. *Gene* **110,** 119–122 (1992).
110. Thomas, B. J. & Rothstein, R. Elevated recombination rates in transcriptionally active DNA. *Cell* **56,** 619–630 (1989).
111. Akter, R. *et al.* Islet Amyloid Polypeptide: Structure, Function, and Pathophysiology. *J. Diabetes Res.* **2016,** (2015).
112. Westermark, P., Andersson, A. & Westermark, G. T. Islet amyloid polypeptide, islet amyloid, and diabetes mellitus. *Physiol. Rev.* **91,** 795–826 (2011).

113. Mukherjee, A., Morales-Scheihing, D., Butler, P. C. & Soto, C. Type 2 diabetes as a protein misfolding disease. *Trends Mol. Med.* **21,** 439–449 (2015).

7. Supplementary material

Table 7.1 Plasmids used in this study.

Description	Features	Source
pRS304	*Integrative TRP1 amp^R*	Sikorski and Hieter[94]
p304_pphIAPP	*Integrative TRP1 amp^R GAL1 ^{promoter}-pphIAPP-GFP*	This study
p304_phIAPP	*Integrative TRP1 amp^R GAL1 ^{promoter}-phIAPP-GFP*	This study
p304_hIAPP	*Integrative TRP1 amp^R GAL1 ^{promoter}-hIAPP-GFP*	Menezes *et al*., unpublished
pRS306	*Integrative URA3 amp^R*	Sikorski and Hieter[94]
p306_pphIAPP	*Integrative URA3 amp^R GAL1 ^{promoter}-pphIAPP-GFP*	This study
p306_phIAPP	*Integrative URA3 amp^R GAL1 ^{promoter}-phIAPP-GFP*	This study
p306_hIAPP	*Integrative URA3 amp^R GAL1 ^{promoter}-hIAPP-GFP*	Menezes *et al*., unpublished
pRS426	*2μ URA3 amp^R*	Christianson *et al.*[109]
p426_pphIAPP	*2μ URA3 amp^R GAL1 ^{promoter}-pphIAPP-GFP*	Menezes, *et al*., unpublished
p426_phIAPP	*2μ URA3 amp^R GAL1 ^{promoter}-phIAPP-GFP*	Menezes, *et al*., unpublished
p426_hIAPP	*2μ URA3 amp^R GAL1 ^{promoter}-hIAPP-GFP*	Menezes *et al*., unpublished

Table 7.2 Yeast Strains used in this study.

Yeast Strain	Description	Reference
W303.1A	MATa *can1-100 his3-11,15 leu2-3,112 trp1-1 ura3-1 ade2-1*	Thomas and Rothstein[110]
W303.1A_*TRP1*	W303.1A *trp1-1::TRP1**	Menezes *et al.*, unpublished
W303.1A_ pphIAPP_Trp$_1$	W303.1A *trp1::GAL1pphIAPP-GFP_TRP1**	This study
W303.1A_pphIAPP_Trp$_2$	W303.1A *trp1::GAL1pphIAPP-GFP_TRP1**	This study
W303.1A_ phIAPP_Trp$_1$	W303.1A *trp1::GAL1phIAPP-GFP_TRP1**	This study
W303.1A_ phIAPP_Trp$_2$	W303.1A *trp1::GAL1phIAPP-GFP_TRP1**	This study
W303.1A_hIAPP_Trp	W303.1A *trp1::GAL1hIAPP-GFP TRP1**	Menezes *et al.*, unpublished
W303.1A_*URA3*	W303.1A *ura3-1::URA3**	Menezes *et al.*, unpublished
W303.1A_pphIAPP_Ura$_1$	W303.1A *ura3-1::GAL1pphIAPP-GFP URA3**	This study
W303.1A_pphIAPP_Ura$_2$	W303.1A *ura3-1::GAL1pphIAPP-GFP URA3**	This study
W303.1A_phIAPP_Ura$_1$	W303.1A *ura3-1::GAL1phIAPP-GFP URA3**	This study
W303.1A_phIAPP_Ura$_2$	W303.1A *ura3-1::GAL1phIAPP-GFP URA3**	This study
W303.1A_hIAPP_Ura	W303.1A *ura3-1::GAL1hIAPP-GFP URA3**	Menezes *et al.*, unpublished
W303.1A_ pphIAPP_Trp-Ura	W303.1A *trp1::GAL1pphIAPP-GFP_TRP1 ura3-1::GAL1pphIAPP-GFP URA3**	This study
W303.1A_phIAPP_ Trp-Ura	W303.1A *trp1::GAL1phIAPP-GFP_TRP1 ura3-1::GAL1phIAPP-GFP URA3**	This study
W303.1A_ hIAPP_Trp-Ura	W303.1A *trp1::GAL1hIAPP-GFP_TRP1 ura3-1::GAL1hIAPP-GFP URA3**	Menezes *et al.*, unpublished
W303.1A <pphIAPP_GFP>	W303.1A pRS416_ *GAL1pphIAPP-GFP*	Menezes *et al.*, unpublished
W303.1A <phIAPP_GFP>	W303.1A pRS416_ *GAL1phIAPP-GFP*	Menezes *et al.*, unpublished
W303.1A <hIAPP_GFP>	W303.1A pRS416_ *GAL1hIAPP-GFP*	Menezes *et al.*, unpublished
W303.1A <pphIAPP>	W303.1A pRS416_ *GAL1pphIAPP*	Menezes *et al.*, unpublished

*Integrative constructions

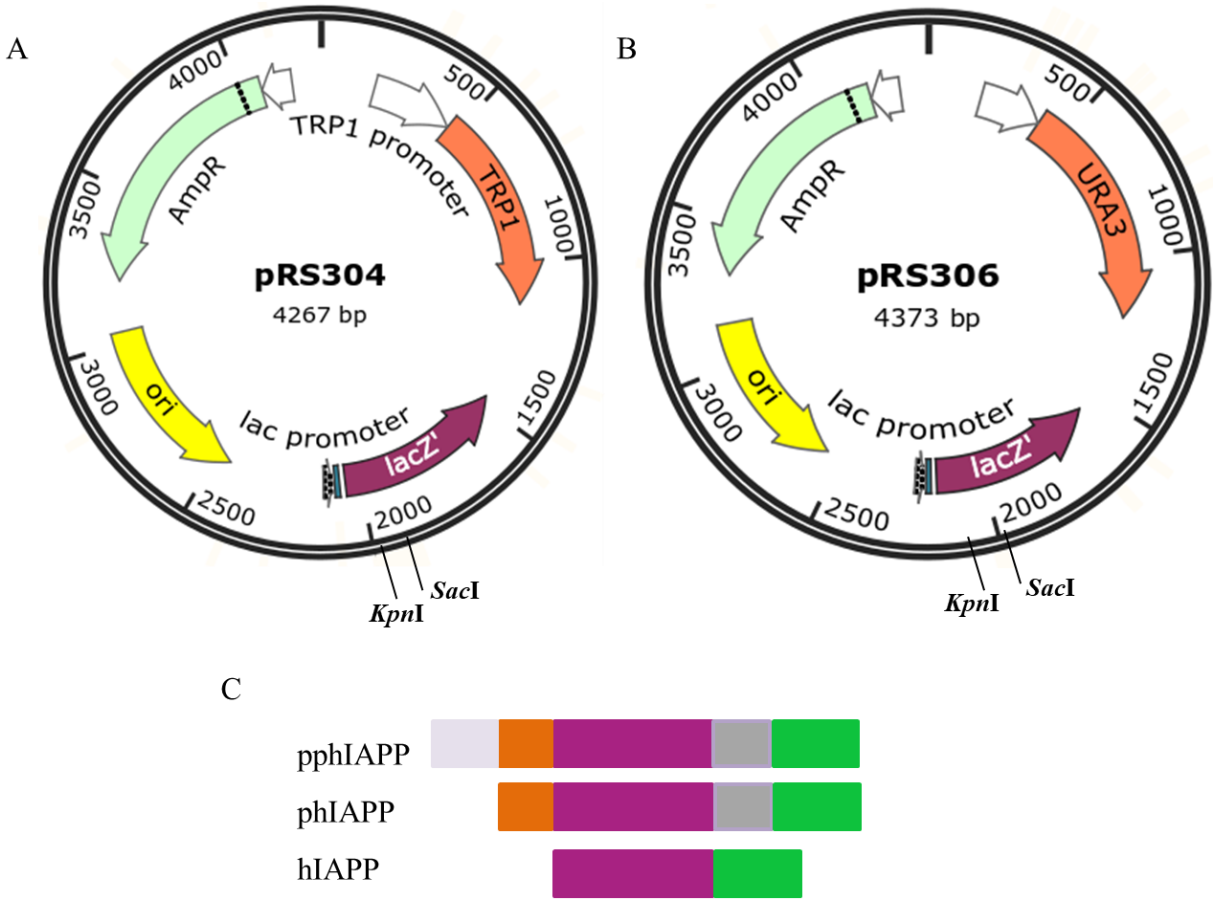

Figure 7.1 Schematic representation of the constructions to express integrative versions of hIAPP in yeast. A) Diagram of the pRS304 and B) pRS306 vectors designed by the SnapGene software (rom GSL Biotech; available at snapgene.com) with the indication of the main features of the vector and the *Kpn*I and *Sac*I restriction sites. C) Schematic representation of pphIAPP, phIAPP and hIAPP with the indication of processed amino acid sequences (grey and orange) and the GFP tag (green). Ori – replicatin origin; AmpR – ampicillin resistance gene (encoding for β-lactamase).

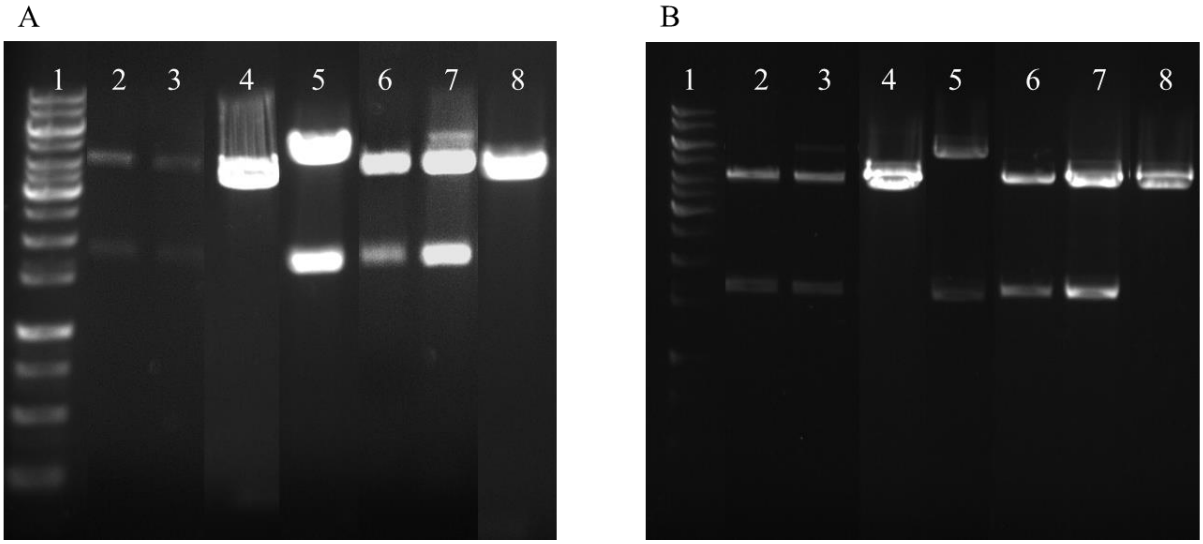

Figure 7.2 Restriction analysis of integrative constructions. The DNA were digested with *Sac*I/*Kpn*I and resolved in a 1% agarose gel. A) Lanes 1 – Molecular weight marker (GeneRuler 1 kb DNA Ladder); 2 – pphIAPP_Trp$_1$; 3 – pphIAPP_Trp$_2$; 4 – pRS304; 5 – p426_pphIAPP; 6 – pphIAPP_Ura$_1$; 7 – pphIAPP_Ura$_2$; 8 – pRS306. B) Lanes 1 – Molecular weight marker; 2 – phIAPP_Trp$_1$; 3 – phIAPP_Trp$_2$; 4 – pRS304; 5 – p426_phIAPP; 6 – phIAPP_Ura$_1$; 7 – phIAPP_Ura$_2$; 8 – pRS306.

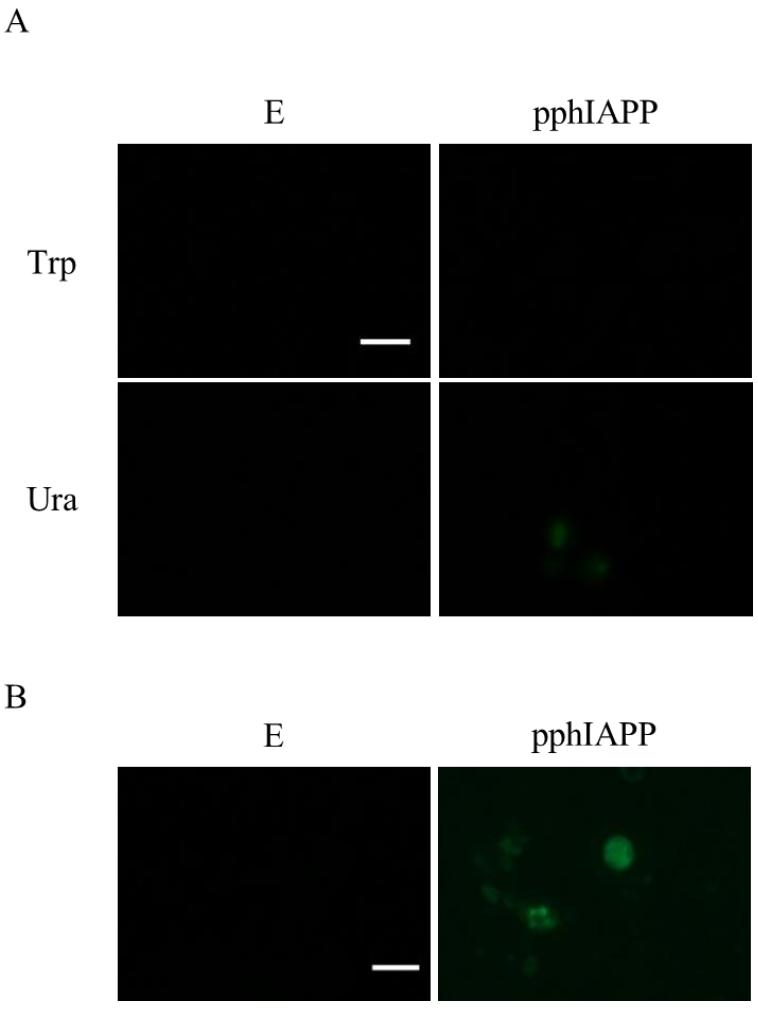

Figure 7.3 Fluorescence microscopy of yeast cells expressing pphIAPP. Cells were first grown in raffinose media and IAPP expression was induced with galactose for 6 h. A) Cells encoding a copy of pphIAPP from the Trp and Ura sets. The fluorescence is undetectable. B) Cells encoding two integrated copies of pphIAPP. Fluorescence of cells was residual. Scale bar= 10 μm. Trp – tryptophan; Ura – uracil; E – Empty vector; pphIAPP – pre pro human IAPP.